



Indian Ocean marine biogeochemical variability and its feedback on simulated South Asia climate

Dmitry V. Sein¹, Anton Y. Dvornikov², Stanislav D. Martyanov², William Cabos³,
Vladimir A. Ryabchenko², Matthias Gröger⁴, Daniela Jacob⁵, Alok Kumar Mishra⁶, and
Pankaj Kumar⁶

¹Alfred Wegener Institute, Helmholtz Centre for Polar and Marine Research, Bremerhaven, Germany

²Shirshov Institute of Oceanology, Russian Academy of Sciences, Moscow, Russia

³Departamento de Física y Matemáticas, Universidad de Alcalá, Alcalá de Henares, Madrid, Spain

⁴Department of Physical Oceanography and Instrumentation, Leibniz Institute for
Baltic Sea Research, Warnemünde, Rostock 18119, Germany

⁵Climate Service Center Germany (GERICS), Hamburg, Germany

⁶Department of Earth and Environmental Sciences, Indian Institute of
Science Education and Research Bhopal, India

Correspondence: Dmitry V. Sein (dmitry.sein@awi.de)

Received: 18 July 2021 – Discussion started: 13 September 2021

Accepted: 3 January 2022 – Published: 13 April 2022

Abstract. We investigate the effect of variable marine biogeochemical light absorption on Indian Ocean sea surface temperature (SST) and how this affects the South Asian climate. In twin experiments with a regional Earth system model, we found that the average SST is lower over most of the domain when variable marine biogeochemical light absorption is taken into account, compared to the reference experiment with a constant light attenuation coefficient equal to 0.06 m^{-1} . The most significant deviations (more than $1\text{ }^{\circ}\text{C}$) in SST are observed in the monsoon season. A considerable cooling of subsurface layers occurs, and the thermocline shifts upward in the experiment with the activated biogeochemical impact. Also, the phytoplankton primary production becomes higher, especially during periods of winter and summer phytoplankton blooms. The effect of altered SST variability on climate was investigated by coupling the ocean models to a regional atmosphere model. We find the largest effects on the amount of precipitation, particularly during the monsoon season. In the Arabian Sea, the reduction of the transport of humidity across the Equator leads to a reduction of the large-scale precipitation in the eastern part of the basin, reinforcing the reduction of the convective precipitation. In the Bay of Bengal, it increases the large-scale precipitation, countering convective precipitation decline. Thus, the key impacts of including the full biogeochemical coupling with corresponding light attenuation, which in turn depends on variable chlorophyll *a* concentration, include the enhanced phytoplankton primary production, a shallower thermocline, and decreased SST and water temperature in subsurface layers, with cascading effects upon the model ocean physics which further translates into altered atmosphere dynamics.

1 Introduction

The vulnerability and the ability of society and natural systems to adapt to the impact of climate change vary significantly according to geographic region and population. The Indian subcontinent and adjacent area, where a fifth of humanity lives, is one of the regions where the impacts are substantial both in the present time and future climate projections (Turco et al., 2015; Szabo et al., 2016). The strongest impacts are related to changes in the intensity and frequency of extreme events, such as floods, droughts, tropical cyclones, storm surges, phytoplankton blooms, ocean heat waves, avalanches, etc. which can inflict significant damage on ecosystems, human populations, infrastructure and property (IPCC AR5, 2014).

Atmospheric extreme events contribute to the emergence of extreme situations in the ocean and vice versa. For example, the strengthening of the southwestern monsoon in the Arabian Sea (ASF) leads to abnormal coastal upwelling. It increased mixing of the upper ocean layer, and the subsequent supply of nutrients into the upper layer from the deep ocean favors anomalous blooms of phytoplankton (Ryabchenko et al., 1998). In turn, the changes in sea surface temperature (SST) and surface fluxes of heat and momentum caused by monsoons can feedback to atmospheric circulation. Another example of the relationship between atmospheric and oceanic processes is associated with river runoff and nutrient loading, which is projected to be maximal in southern and eastern Asia due to population growth and increased industrialization (Seitzinger et al., 2002). It was stated that the estuarine ecosystem experiences a complete change in terms of phytoplankton during monsoons (De et al., 2011) and that the eastern Indian coast is affected by localized eutrophication which directly influences the nutrient level of coastal water and phytoplankton abundance (Choudhury and Pal, 2010). Recent assessments (Sattar et al., 2014) of the impact of food production upon the river flux of nutrients into the Bay of Bengal (BBF) coastal waters in the past and the future show that the coastal eutrophication potential is high in the Bay of Bengal, thus elevating the risk for oxygen deficiencies (D'Asaro et al., 2020). The above examples of interactions between atmospheric and oceanic processes underscore the need to create a unified high-resolution modeling system for the region to be able to study these interactions in detail.

Earth system models (ESMs) are very effective tools for the study of complex systems and associated mechanisms in climate and environmental sciences in the past and future, driven by assumptions on the evolution of climate change (Taylor et al., 2012). However, they usually lack the resolutions that are necessary for regional studies. Regional climate models (RCMs) are used to translate the global climate information generated by ESMs down to regional scales at a higher resolution. RCMs take the initial conditions and time-dependent boundary conditions from the global models and

provide dynamically downscaled climate information within the region of interest (Giorgi, 2006).

We have implemented a new version of the high-resolution regional Earth system model (RESM) ROM (Sein et al., 2015) for South Asia and the northern Indian Ocean (IO). The model includes ocean, atmosphere, hydrological cycle and marine biogeochemistry components. Such a modeling system is required for the study of extreme events in the atmosphere and the ocean in the India region, for seasonal and decadal predictions, climate change projections, and advanced monsoon modeling.

In this study, we will use the model to assess the impact of a fully coupled interactive marine biogeochemical model upon the simulation of the present climate over the Indian subcontinent and the adjacent ocean using the South Asia CORDEX domain (CORDEX – Coordinated Regional Climate Downscaling Experiment, <https://cordex.org/domains/region-6-south-asia-2>, last access: 1 July 2021). Monsoon dynamics are sensitive to changes in SSTs and so a model representing the Indian Ocean should involve all relevant processes to control the heat budget of the near-surface ocean. We focus here on the impact of variable chlorophyll concentration on SSTs and how this feeds back on climate. A number of studies focused on the investigation of the marine biogeochemistry impact upon physical properties of the ocean showed that the general scheme is as follows: the presence of phytoplankton leads to the warming of the ocean upper layer and the cooling of subsurface layers (e.g., Nakamoto et al., 2000; Lengaigne et al., 2007; Park et al., 2014a, b). Nevertheless, in some circumstances, the presence of phytoplankton, as reported by Nakamoto et al. (2001), Manizza et al. (2005) and Park et al. (2014b), may lead to the cooling of the surface layer as well due to enhanced upwelling of cold subsurface water in the eastern equatorial Pacific. Still, the warming of the eastern equatorial Pacific due to the influence of biological productivity was reported by Lengaigne et al. (2007), who compared the fully coupled ocean–atmosphere–biogeochemistry model experiment with the fixed-chlorophyll model experiment. They also discussed the inconsistency between the results of forced ocean models and the fully coupled models, suggesting that the impact of marine biogeochemistry upon SST and corresponding cooling or warming is related to the way radiation is treated in the control experiments. The climate variability in the Indian Ocean was studied by Park and Kug (2014), who also showed that the presence of chlorophyll increases the mean SST due to biological heating. Therefore, a significant number of published studies on biogeochemical influence upon ocean physics have shown that taking into account phytoplankton's presence while computing the penetration of the short-wave solar radiation into the water leads to the warming of the surface layer and cooling of subsurface layers of the ocean. One of the main approaches in those studies was setting the phytoplankton concentration equal to zero (a reference experiment, so-called “dead ocean”), to a constant

value (studying the influence of phytoplankton upon ocean physics, but not vice versa), or using a fully interactive simulated phytoplankton concentration affecting the shortwave radiation (SWR) absorption when all possible feedbacks between physical and biogeochemical models are taken into account (e.g., Manizza et al., 2005; Lengaigne et al., 2007). Our current research differs in that we do not investigate the influence of phytoplankton upon ocean physics in general but investigate how the spatial and temporal variability of marine biogeochemistry affects the regional climate. Given the changing climate reality, such a question seems reasonable and worth discussion. Should the variability of marine biogeochemistry be taken into account when performing ESM climatic predictions? Which part of the climatic system will be affected, and which will not?

To answer these questions, we compare two simulations carried out with our RESM. These two simulations differ only in the influence of the ocean biochemistry module on the shortwave solar radiation penetration into the ocean. In the first simulation, we use a constant in time and space light attenuation coefficient corresponding to a Jerlov IB water type (Jerlov, 1976; Paulson and Simpson, 1977). Although such a value of the attenuation coefficient may implicitly include the impact of phytoplankton, it absolutely neglects its spatial and temporal variability. In the second simulation, we introduce the full spatial and temporal variability of marine biogeochemical feedback by calculating the attenuation coefficient using the phytoplankton concentration simulated by the ocean biogeochemistry module following Gröger et al. (2013).

It is worth mentioning that many previous studies investigating the role of phytoplankton feedback on climate were based mainly on global models, i.e., either global marine biogeochemistry models or global coupled atmosphere–ocean biogeochemistry models. These models do not account well for small-scale dynamics and thus often yield a spatially smoothed picture of phytoplankton dynamics. In this study, both the atmospheric as well as the oceanic components are in a resolution that fully provides the added value of regionalization compared to global models. This has been demonstrated previously for the North Atlantic as well as the NW European shelf seas (Sein et al., 2015, 2020).

Finally, it is well known that ongoing climate change will reduce the mixed-layer depth in many ocean regions together with a decline of ocean productivity (Steinacher et al., 2010; Fu et al., 2016). Furthermore, changes in atmospheric nutrient depositions turn out to be a driver of biological productivity in many oligotrophic regions (Myriokefalitakis et al., 2020). The changes in production are likely to alter the water chlorophyll concentration of the upper ocean and thus on SST. The impacts can not be simulated with models using Jerlov-type light attenuation, and so the role of phytoplankton in climate change projections is more or less unexplored.

The objectives of this paper can be summed as follows:

1. to evaluate the ability of our model to reproduce the present climate in the South Asia CORDEX region both in the ocean and the atmosphere;
2. to evaluate the quality of corresponding simulated physical and biogeochemical characteristics in the northern part of the Indian Ocean;
3. to assess the impact of the full spatial and temporal variability of marine biogeochemistry's feedback upon the simulated regional climate, both in the atmosphere and the ocean.

The layout of the present paper is as follows. In Sect. 2 a description of the coupled modeling system is presented. Section 3 is focused on the verification of the developed RESM. Section 4 contains some discussion. Conclusions are presented in Sect. 5.

2 Methods

The oceanic component of ROM is the global Max Planck Institute Ocean Model (MPIOM: Marsland et al., 2002; Jungclaus et al., 2013), which is coupled to the REgional atmospheric MOdel (REMO: Jacob, 2001a, b) via the OASIS coupler. ROM also includes as modules the Hamburg Ocean Carbon Cycle model (HAMOCC: Ilyina et al., 2013), and the Hydrological Discharge model (HD: Hagemann and Dumenil, 1998). MPIOM provides the possibility to refine the grid resolution in the region of interest and to avoid the lateral boundary conditions in the ocean while performing calculations. Another feature of the ROM system is that the coupling between the ocean and the atmosphere is implemented only at the chosen subdomain. At the same time, outside this region, MPIOM calculates heat, freshwater and momentum fluxes from atmospheric fields taken from the same global model used for REMO boundary conditions. A detailed description of ROM can be found in Sein et al. (2015).

In this work, we use for REMO the slightly enlarged South Asia CORDEX domain (<http://www.cordex.org>, last access: 1 July 2021), while for MPIOM the global mesh has a variable horizontal resolution which reaches up to 15 km inside the coupled region and ranges from 23.3 to 24.5 km in the part of the Indian Ocean included in this domain (Fig. 1). MPIOM has 40 vertical z -coordinate levels with the following thicknesses (in meters): 16, 10, 10, 10, 10, 10, 13, 15, 20, 25, 30, 35, 40, 45, 50, 55, 60, 70, 80, 90, 100, 110, 120, 130, 140, 150, 170, 180, 190, 200, 220, 250, 270, 300, 350, 400, 450, 500, 500, 600. The model is driven by atmospheric data from a CMIP5 20th century simulation with the MPI-ESM LR setup.

For this study, we perform two present-time simulations using ROM. The two simulations (labeled as INDJ and INDB hereafter) are almost identical and differ only in the parameterization of the attenuation of SWR penetrating into the ocean. In the INDJ experiment, we use a constant in time and

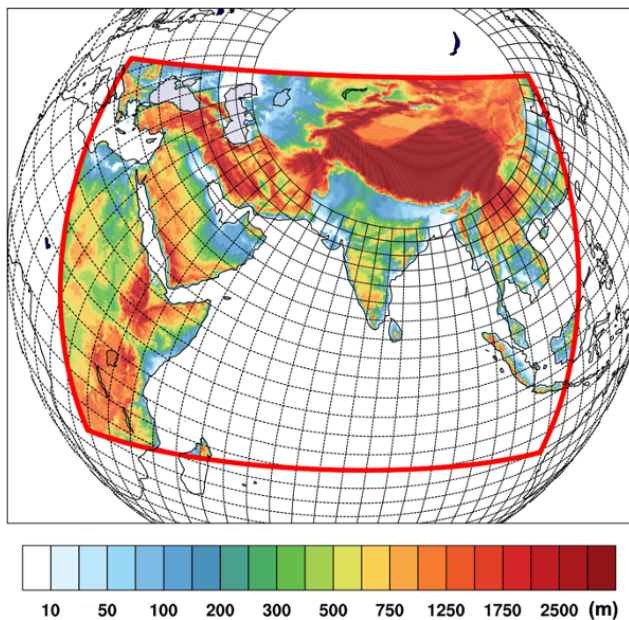


Figure 1. ROM configuration. The red frame shows the coupled ocean–atmosphere CORDEX domain. The black lines indicate the grid of the MPIOM/HAMOCC models (only every 12th line is shown). Color scale represents orography.

space light attenuation coefficient equal to 0.06 m^{-1} which corresponds to Jerlov IB water type (Jerlov, 1976; Paulson and Simpson, 1977). Although this parameterization implicitly includes the impact of phytoplankton, it neglects its spatial and temporal variability and has several shortcomings. Firstly, the impact of the dynamics of phytoplankton blooms on the light climate is completely neglected, which is highly problematic in regions which are subject to a strong seasonal cycle and in regions with strongly varying nutrient supply. Secondly, coastal characteristics, especially in front of large rivers with a high nutrient load and limited exchange with the open ocean, are not resolved, which is, however, crucial in high-resolution downscaling simulations. This experiment was performed for the period 1920–2005, the first 30 years being an adjustment period. Initial conditions for the biogeochemical module were taken from MPIOM/HAMOCC long-term simulations (Gröger et al., 2013). For the ocean and atmosphere, the initial conditions were taken from previous spin-up simulations: 50 years MPIOM stand-alone run plus 2×40 years coupled MPIOM/REMO simulations with ERA-Interim forcing.

In the second simulation (INDB), which starts from the beginning of the year 1950 of the INDJ experiment, we introduce the full spatial and temporal variability of marine biogeochemical feedback by calculating the attenuation coefficient using the phytoplankton concentration simulated by the ocean biogeochemistry module as proposed by Gröger et al. (2013). Hence, the presence of a strong local phytoplankton bloom in the surface layer will increase the heat

absorption in the upper layers and decrease it in deeper layers compared to a no-bloom period, with cascading feedback on the thermohaline structure of the water column and heat flux between the ocean and the atmosphere. Due to these reasons, the effect of seasonally and locally varying phytoplankton concentration can be expected to be important in regional climate studies. Including the full variability of the marine biogeochemical feedback, as is done here, is not a common practice in climate simulations, as it requires online coupling to a biogeochemistry model which leads to a 3-fold consumption of CPU hours compared to an uncoupled model running with Jerlov water types.

We compare the calculation results for both experiments (INDJ and INDB) with the best observational data sets to date for the region under consideration: they include oceanographic data compiled in the World Ocean Atlas 2013 (WOA13, Levitus et al., 2014) and the satellite data from the Sea-viewing Wide Field-of-view Sensor (SeaWiFS) and Moderate-resolution Imaging Spectroradiometer (MODIS) Terra. The WOA13 is a set of climatological-mean, gridded fields of oceanographic variables based on in situ measurements from a wide variety of sources. Global, decadal averages of temperature, salinity, oxygen and nutrients are provided for monthly, seasonal and annual averaging periods on 102 standard depth levels from 0 to 5500 m, and at 0.25° (temperature, salinity) and 1° (all variables) horizontal resolutions. We do not use the latest edition of WOA18 (Boyer et al., 2018) for the following reasons: (1) WOA13 is widely used in the scientific literature and thus can be easily compared to other studies that use the same reference, and (2) as stated in the WOA18 description (<https://www.ncei.noaa.gov/data/oceans/woa/WOA18/DOC/woa18documentation.pdf>, last access: 1 July 2021) WOA18 temperature and salinity data are still published as preliminary in order to take advantage of community-wide quality assurance and comments.

From satellite data, we use SeaWiFS chlorophyll data (NASA Goddard Space Flight Center, 2021a) and MODIS Terra chlorophyll data (NASA Goddard Space Flight Center, 2021b), as well as SeaWiFS downwelling diffuse attenuation coefficient data (NASA Goddard Space Flight Center, 2021c). The SeaWiFS instrument was launched on the OrbView-2 satellite in August 1997 and collected data from September 1997 until the end of mission in December 2010. MODIS is a key instrument aboard the Terra (EOS AM) and Aqua (EOS PM) satellites and its set of data records covers the period from 24 February 2000 to present time. From above satellite data we used their gridded fields of 9 km resolution having daily and monthly averaging periods.

Apart from the physical feedback of phytoplankton on SST and successive ocean–atmosphere heat exchange, the production of phytoplankton lowers the local concentration of dissolved inorganic carbon and thus the $p\text{CO}_2$ of the surface water. As a result, the air–sea $p\text{CO}_2$ gradient is altered which in turn feeds back on the air–sea carbon ex-

change. However, as in the overwhelming part of coupled ocean–biogeochemistry–atmosphere models, the air–sea carbon fluxes are passively coupled. Consequently, an increased air-to-sea carbon flux due to a strong phytoplankton bloom is not communicated to the atmosphere. Consequently, unlike water $p\text{CO}_2$, atmospheric $p\text{CO}_2$ does not change but is prescribed during the whole simulation. In conclusion, the only way phytoplankton influences the atmosphere is by its impact on SST and subsequent heat fluxes.

3 Results

3.1 Ocean

For validation of the model results, we use the temperature, salinity, dissolved nitrates and dissolved phosphates data from the WOA13, and chlorophyll concentration from the satellite data (SeaWiFS and MODIS Terra).

According to long-term observations of the Indian Meteorological Department, we distinguish the following seasonal periods used for the verification procedure based on the monsoon activity in South Asia and in the northern part of the Indian Ocean:

- DJF: December–February (winter season, northeasterly (NE) winds);
- MAM: March–May (pre-monsoon season);
- JJAS: June–September (monsoon season, southwesterly (SW) winds);
- ON: October–November (post-monsoon season);

In the following, we compare the model results and observations for winter (DJF) and monsoon (JJAS) seasons time-averaged over 1975–2004, since the phytoplankton impact is expected to be maximal during the bloom periods.

3.1.1 Sea surface

Sea surface temperature and salinity (SST and SSS). Figure 2 shows the spatial distribution of the difference between the INDJ and WOA13 SST (Locarnini et al., 2013) and SSS (Zweng et al., 2013) for winter (DJF) and monsoon (JJAS) seasons averaged over the 1975–2004 period. The model generally underestimates the SST, the exception being the region located off the coast of the Somali peninsula. The most considerable deviations in SSS from the WOA13 are observed in the Bay of Bengal, with overestimations by the model in the 0.5‰–2‰ range. The largest discrepancy in SSS occurs in winter (DJF), while in pre-monsoon (not shown) and monsoon seasons, the maximum difference is about 0.5‰ and 1.5‰, respectively. Off the western Indian coast, INDJ shows a somewhat lower SSS than that in the WOA13, with the largest discrepancies occurring in the post-monsoon season and being up to 1‰ (not shown).

Sea surface concentration of dissolved nitrate. HAMOCC somewhat overestimates the surface concentration of nitrates (NO_3), especially during winter (Fig. 2). The strongest deviations are located along the coasts. They are related to uncertainties in nutrient supply originating from rivers and point sources as we apply a rough climatological estimate for external nutrient supply (Gröger et al., 2013). Further from the coasts, the model biases reduce, showing the model's capability to correctly simulate the biogeochemical cycling of the open Indian ocean, which is the primary purpose of this study. Overly high SSTs and overly low nitrate concentrations near the NE Africa and South Arabia coast during the monsoon season may indicate that the model produces an overly weak upwelling in response to the predominant SW wind regime. The agreement between WOA13 (Garcia et al., 2014) and the model varies with depth: at 50 m the main features of the spatial distribution of nitrates are reproduced correctly. The only serious exception is the overestimation of the concentration of nitrates in the post-monsoon season off the southwest coast of India. At a depth of about 100 m the discrepancies become more pronounced, while at 500 m the WOA13 and modeled nitrates are very similar, as the influence of the seasonal ecosystem dynamics upon the distribution of nitrates at such depths becomes small. The maximum deviations in surface nitrate field between the model and WOA13 data occur during the bloom periods (winter and monsoon seasons), while this deviation is minimal in the pre-monsoon season. In general, the modeled annual surface concentration of dissolved nitrate is slightly higher than in WOA13.

Sea surface chlorophyll a concentration. For the validation of the ocean surface chlorophyll *a* concentration, the surface phytoplankton concentration (in carbon units) calculated by HAMOCC was converted into chlorophyll *a* concentration (in mg m^{-3}) using a constant C : Chl ratio equal to 60 gC gChl^{-1} (Ilyina et al., 2013). Figure 3 demonstrates the spatial distribution of modeled (INDJ) and observed (SeaWiFS) surface chlorophyll *a* concentration for winter and monsoon seasons.

It is clear that ROM overestimates the chlorophyll *a* concentration in comparison with SeaWiFS satellite data (NASA Goddard Space Flight Center, 2021a). The model produces lower chlorophyll *a* concentrations in the Arabian Sea under the predominant NE wind regime during the winter monsoon. By contrast, SW winds during the summer monsoon induce the upwelling of nutrients from deeper layers and stimulate primary production. In winter the model simulates enhanced chlorophyll *a* concentrations along the eastern boundary of the Bay of Bengal while showing their decrease during monsoon season. These modeled chlorophyll *a* changes are in accordance with seasonal changes of the wind regime. However, the satellite data show high concentrations during monsoon season in that coastal area that our model

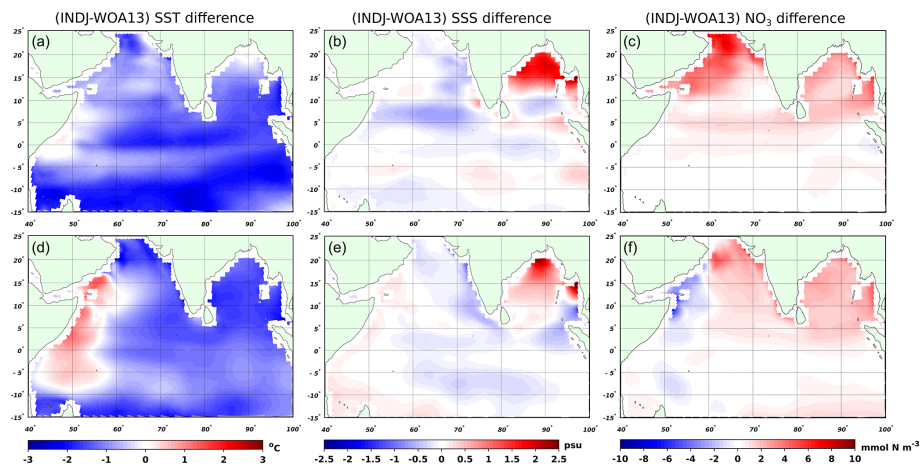


Figure 2. Spatial distribution of the difference between experiment INDJ and WOA13 for SST (a, d), SSS (b, e) and NO_3 in the surface layer (c, f). SST, SSS and NO_3 are time-averaged for the winter season (DJF; a–c) and monsoon season (JJAS; d–f) for the period 1975–2004.

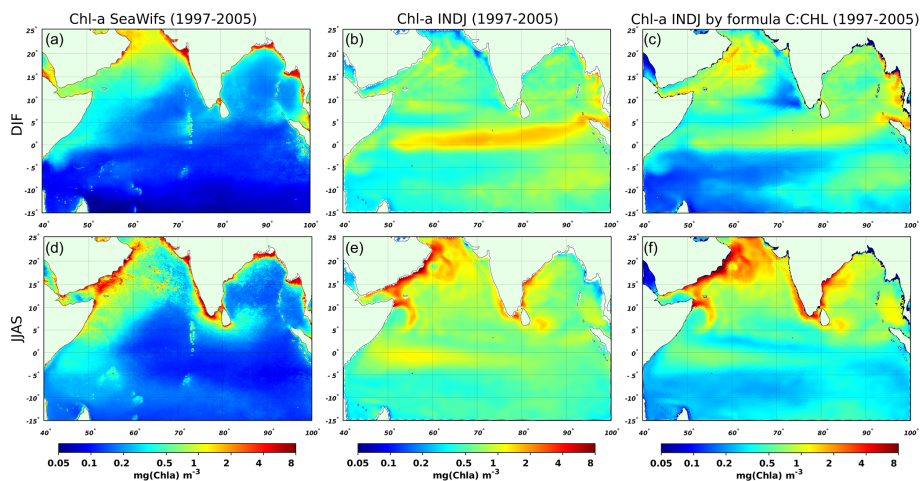


Figure 3. Distribution of surface chlorophyll *a* concentration obtained by the SeaWiFS satellite data (NASA Goddard Space Flight Center, 2021a; a, d), model using a fixed C : Chl ratio (b, e), and using a varying C : Chl ratio as in Anderson et al. (2007) (c, f), for winter (a–c) and monsoon (d–f) climatic seasons.

did not represent. The most plausible explanation for this is a persistently high supply of riverine nutrients around the year which occurs in reality and which is not specified in our model. Another difference between the model and satellite data is the presence of increased chlorophyll *a* concentration zone stretching along the Equator in the model results, especially during the winter season, which is not present in satellite data. A good agreement, both qualitative and quantitative, between the model's winds and ERA5's winds (Fig. 17; see below) suggests that the enhanced model's equatorial surface phytoplankton concentration cannot simply be related to incorrect wind simulation. The problem may be related to the relatively coarse vertical resolution of MPIOM in the upper layer (16 m) together with a simple turbulence closure scheme in MPIOM based on Pacanowski and Philander (1981). The overestimation or underestimation of ocean

productivity along the equatorial divergence zone is a common problem of many ocean general circulation models (e.g., Steinacher et al., 2010). Liu et al. (2013) also reported and discussed significant discrepancies between observed and modeled chlorophyll *a* surface concentrations in the equatorial Indian Ocean in an ensemble of five CMIP5 coupled models. Their analysis showed that all the considered models shared the same structures and deviations in that region. Unfortunately, our RESM also has the same drawback in this really challenging problem.

The overestimation of chlorophyll *a* concentration in the domain may also be explained by a relatively simple description of phytoplankton dynamics in the HAMOCC model. HAMOCC includes only one type of phytoplankton and, as a component of a global climatic model, it was configured to produce realistic global-mean primary production (Ilyina et

al., 2013) but may significantly over- or underestimate some regional features of marine biological productivity. We suppose that this is the main cause of differences between satellite and model results. This also holds for overestimated regional concentration of dissolved nitrate, which is another issue of HAMOCC and other global models (Ilyina et al., 2013).

Another cause of modeled chlorophyll *a* overestimation may be the fixed phytoplankton C : Chl ratio used in the HAMOCC model. As was mentioned above, HAMOCC uses a constant C : Chl ratio equal to 60 gC gChl⁻¹, and this ratio is used herein to convert the modeled surface phytoplankton concentration (expressed in carbon units) into surface chlorophyll *a* concentration (expressed in mg Chl m⁻³) in order to validate the model's results against SeaWiFS satellite data. Nevertheless, as was shown in numerous studies, the phytoplankton C : Chl ratio is very variable, depending on specific phytoplankton species, irradiance level and bloom phase. The values of the C : Chl ratio may be 20–50 at low irradiances and up to 100–200 at high irradiances, as reported by Smith and Sakshaug (1990).

Besides a fixed C : Chl ratio, a functional dependency of C : Chl can be used in some models. For example, in Anderson et al. (2007) such function was used in a biogeochemical model of the Arabian Sea, which includes water temperature and nutrient concentrations as arguments. Figure 3 shows the surface chlorophyll *a* concentration (converted from modeled phytoplankton concentration) calculated with a fixed and variable (Anderson et al., 2007) C : Chl ratio in order to compare it with satellite data and check if a variable phytoplankton C : Chl ratio may give a better agreement with SeaWiFS observations.

As seen from Fig. 3, using the above-mentioned parameterization for phytoplankton variable C : Chl ratio gives better agreement between model and SeaWiFS surface chlorophyll *a* concentration. It should be noted that the constant C : Chl ratio is used in HAMOCC in the photoadaptation process, so, strictly speaking, it is not consistent to use another C : Chl ratio for converting the modeled phytoplankton concentration into chlorophyll *a* concentration, but it is still useful to demonstrate the impact of phytoplankton C : Chl ratio variability upon the model's verification.

A comparison of the HAMOCC surface chlorophyll *a* concentration with satellite data was also carried out for some locations in the Arabian Sea, Somali upwelling area and Bay of Bengal (Fig. 4). The general overestimation of simulated chlorophyll *a* surface concentrations mentioned above is also evident at these locations. However, during several short periods the MODIS's daily-mean climatic concentrations (NASA Goddard Space Flight Center, 2021b) appear to be higher than in the model. The period of analysis presented in Fig. 4 is related to the availability of MODIS Terra (2000–2021) and SeaWiFS (1997–2010) data. Because our simulations span up to 2005, the resulting common period for the model results and satellite data is 1997–2005, which is used

in Fig. 4 to calculate mean values of surface chlorophyll *a* concentration for this period.

3.1.2 Vertical distributions

We have also analyzed the spatially averaged vertical profiles of water temperature, salinity, dissolved nitrate and phosphorus concentration for the northern part of the Indian Ocean (IO) and for the Arabian Sea (ASF) and the Bay of Bengal (BBF) regions (Fig. 5).

As seen from Fig. 6, the simulated vertical distribution of temperature and salinity is in relatively good agreement with WOA13 data. Model results are generally within the standard deviation range of the corresponding WOA13 data in ASF and in IO. However, in BBF the modeled temperature and salinity are out of the standard deviation range. Still, it should be noted that the standard deviation of WOA13 temperature in the whole water column and salinity below 100 m is very small in these areas due to the scarcity of observations. The same is true for the vertical distribution of nutrients (Fig. 7).

3.1.3 Mixed-layer depth

A possible way to analyze the impact of biology on the water column is how it affects mixing. Hence, we calculated the mixed-layer depth (MLD) according to the 0.2 °K criterion and compared it directly to the observation-based mixed-layer depth climatology provided by de Boyer Montégut al. (2004) (Fig. 8). During the SW monsoon season (JJAS) ROM simulates a deeper MLD in a narrow band along the coast of Somalia compared with observational data (Fig. 8a, upper panel). Due to a higher horizontal resolution of the ocean module MPIOM (up to 15 km), ROM can generally better reproduce small-scale structures compared to the data of de Boyer Montégut al. (2004), which has horizontal resolution of only 2° and where small-scale structures may be less pronounced. A big mismatch is seen in the eastern Bay of Bengal where INDJ simulates a very deep (> 70 m) MLD which is not seen in the observations. This points to a systematic overestimation of the MLD in this area. However, the difference between INDB and INDJ (Fig. 8b, left) shows that this bias is substantially reduced when ROM takes into account the explicit heat absorption by modeled phytoplankton.

During monsoon season (Fig. 8a, JJAS) the MLD deepens in the southern part of the domain in both ROM and observations. However, in the observations, the zone of deep mixing expands more northward compared to ROM.

During the winter season (DJF), the observational data set shows much lower spatial variation of the MLD than in the INDJ experiment (Fig. 8a, lower panel). Partly, this is expected due to the coarse resolution of the observational data set. However, it is obvious that in both the Arabian Sea as well as in the Bay of Bengal, ROM seems to overestimate the MLD, whereas in the southern part of the domain, where

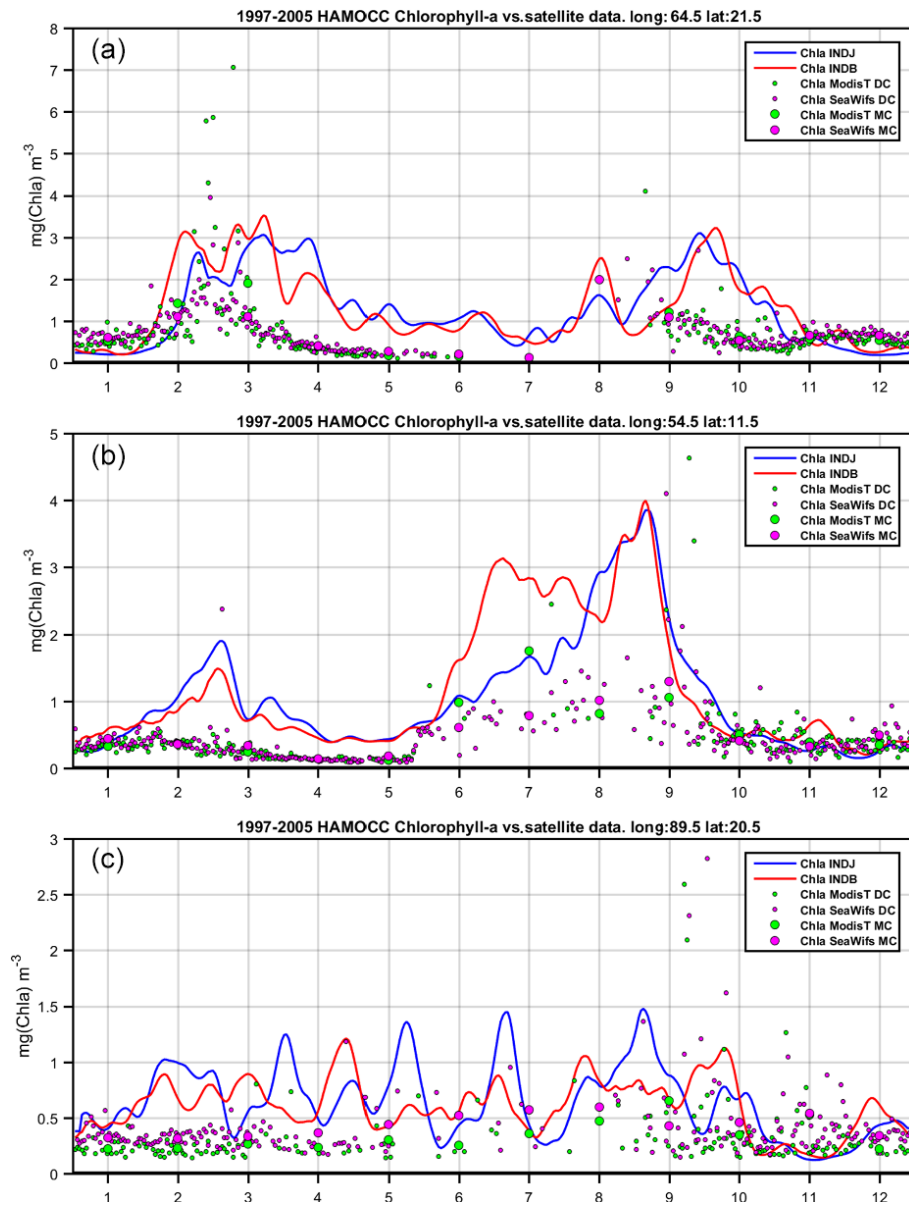


Figure 4. Comparison of the simulated (INDJ and INDB) and observed (SeaWiFS, MODIS Terra) surface chlorophyll *a* concentration in the Arabian Sea (a), Somali upwelling area (b) and the Bay of Bengal (c). DC and MC – daily-mean and monthly-mean climatic averaging of satellite data for the period 1997–2005, respectively. The blue and red curves (Chl *a* INDJ and Chl *a* INDB) are daily-mean climatic averaging of modeled surface chlorophyll *a* concentration for the period 1997–2005.

the MLD is generally shallower, the differences are less pronounced. In the northern Indian Ocean, as seen in Fig. 8b, the MLD is much shallower in the simulation with explicit consideration of heat absorption by simulated phytoplankton (INDB) compared to the experiment with the constant attenuation coefficient (INDJ). Therefore the differences with the observational data are substantially reduced in INDB compared to INDJ.

3.1.4 Impact of the fully coupled marine biogeochemical variability

Impact on the water temperature and salinity. Here we investigate the impact of variable chlorophyll *a* concentration when using the corresponding light attenuation parameterization (see Gröger et al. (2013) for details) upon the main oceanic variables by comparing the experiments INDB and INDJ. The vertical distribution of temperature, salinity, dissolved nitrate and phosphate for different regions of the model domain was already presented in Figs. 6–7 for both

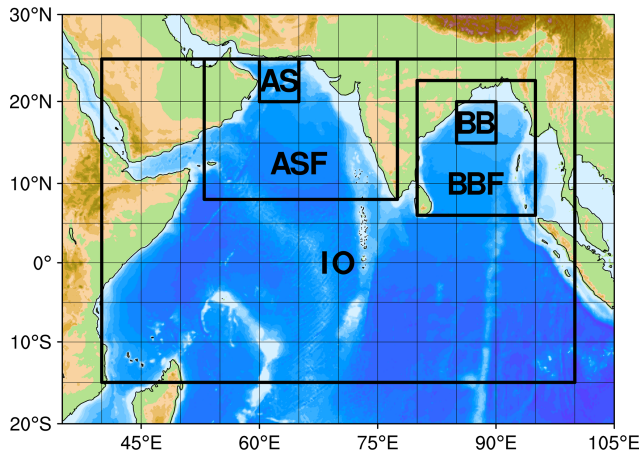


Figure 5. Regions over which spatial average is computed for the vertical profiles of fields (temperature, salinity and nutrients). Acronyms as used for further analysis: IO – Indian Ocean, ASF – Arabian Sea full, AS – Arabian Sea box, BBF – Bay of Bengal full, BB – Bay of Bengal box.

experiments. Figure 9 shows the spatial distribution of the difference of the climatological (1975–2004) values of the SST and corresponding standard deviation of the two model runs (INDB–INDJ). In winter (DJF), the use of the light attenuation parameterization based on simulated chlorophyll concentration in INDB leads to a lower SST, which becomes up to 1 °C colder in the northern part of the Arabian Sea. The exceptions are the areas near the southwestern coast of India, the northwestern coast of Indonesia and the eastern part of the Andaman Sea, where an insignificant SST increase which does not exceed 0.1 °C can be found. In monsoon season (JJAS) the difference in SST between the two runs is even more pronounced, especially in the northern part of the Arabian Sea and along the eastern coast of India. SST in INDB is also characterized by stronger variability, with a standard deviation of SST approximately 0.3 °C higher than in INDJ.

When averaging over the annual period (not shown), SST in INDB is also slightly lower and its standard deviation is higher than in INDJ.

Figure 10 shows the spatial distribution of the differences (INDB–INDJ) in DJF and JJAS mean SSS and standard deviation for the same period (1975–2004). Our results show that in all seasonal climatic averages the SSS difference between INDB and INDJ experiments is not strongly pronounced and does not generally exceed 0.2‰. The most significant changes in SSS occur in the Bay of Bengal. Figure 10 also shows that the standard deviation in the two simulations is quite similar, except for the northern part of the Bay of Bengal where the INDB run showed larger seasonal deviations relative to the INDJ experiment.

Impact on the primary production and dissolved nitrate. This is shown in Fig. 11 where the differences in depth-integrated modeled phytoplankton primary production (PP)

and surface concentration of dissolved nitrate (NO_3) are presented. It can be seen that the PP is higher in the INDB experiment during the main phytoplankton bloom periods (DJF and JJAS). The surface concentration of dissolved nitrates is generally lower in the INDB than in the INDJ experiment. It is especially apparent on the Arabian Sea and agrees well with the increased PP since nutrients are consumed more intensively in the surface layer.

Impact on water temperature in the ocean upper layers. To compare the simulated water temperature in the ocean upper layers (up to 100 m depth), we select two complementary regions, where the largest SST difference between INDB and INDJ are found (designated in Fig. 5 as AS: 60–65° E, 20–25° N and BB: 85–90° E, 15–20° N). Figure 12 shows the DJF and JJAS vertical profiles of water temperature (T), SWR and phytoplankton concentration (Phyt) for the two experiments averaged over the regions AS, BB and IO. We note a significant cooling of subsurface layers in INDB compared to INDJ.

Thermocline dynamics. Thermocline dynamics is among the most important factors mediating the temporal and spatial shape of phytoplankton blooms and their feedback on climate. On the one hand, it acts as a barrier for the vertical exchange between nutrient-depleted surface waters and nutrient-enriched waters from deeper layers and can limit biological productivity. On the other hand, a strong thermocline can effectively reduce the local mixed-layer depth and allow phytoplankton to persist longer within the euphotic layer, thereby increasing the growth rate of marine algae. Moreover, the thermocline has a temperature-mediating effect, with a shallower thermocline allowing the surface layer to faster adapt to atmospheric temperatures (e.g., Gröger et al., 2015). The inclusion of phytoplankton in the radiative heat transfer equation alters the vertical distribution of heat absorption and thus influences the thermocline dynamics. In the following, we compare the thermocline dynamics between the two model runs INDJ and INDB (Fig. 13). A comparison of both runs with WOA13 data is also discussed here.

Data generally tend to be sparse in open-ocean regions with less dense measuring campaigns like the Indian Ocean. Then, caution should be applied when interpreting thermocline dynamics derived from sparse gridded data sets like WOA. Therefore, we do not provide a quantitative validation here but rather discuss the processes underlying the spatial pattern.

Both simulations and WOA data show distinct gradients in thermocline depth (defined here as maximal temperature gradient in the water column). During the monsoon season (Fig. 13a) the thermocline shoals to values smaller than 25 m along the northern coast of the Arabian Sea and along the Indian coast where moisture-carrying SW monsoon winds cause a positive $P-E$ flux and maintain a vigorous runoff (Ramesh and Krishnan, 2005). Off the Somali coast and further offshore, the strong SW monsoonal winds lead to a deepening of the thermocline in wide areas of the open ocean. In

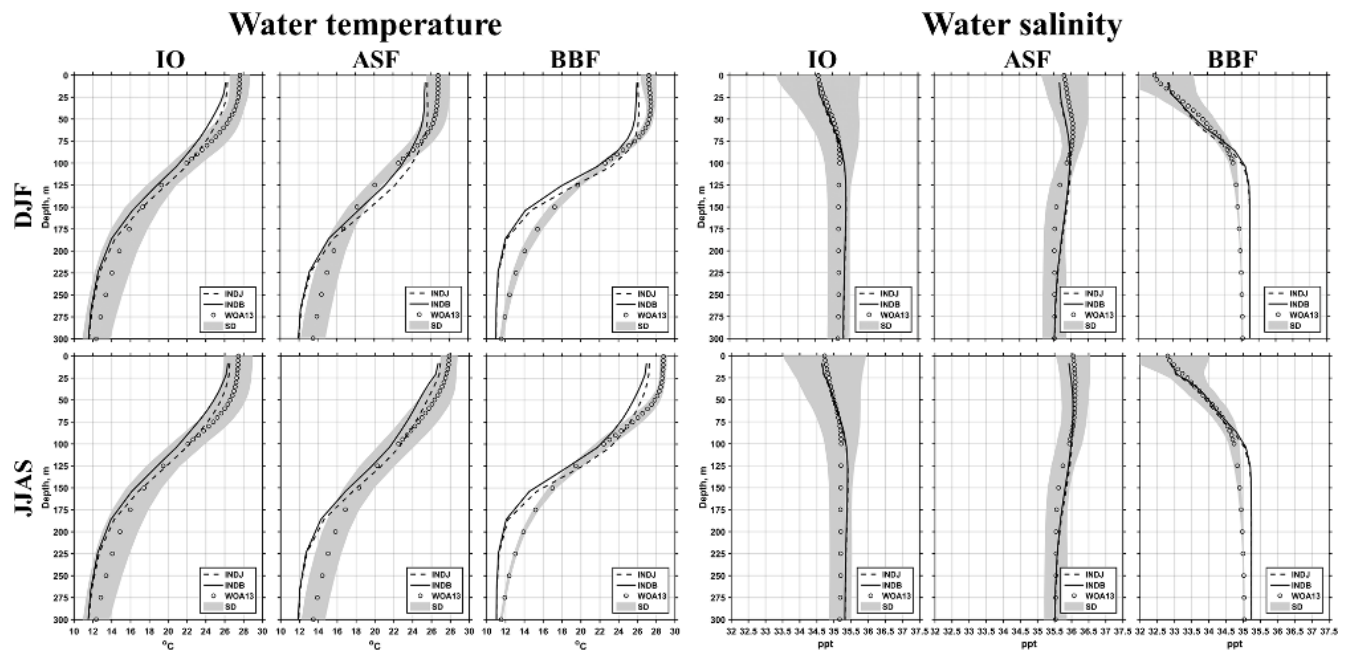


Figure 6. Vertical profiles of water temperature and salinity time-averaged seasonally (DJF, JJAS) for the period 1975–2004. INDJ and INDB designate the model runs. WOA13 designates the climatic data from the World Ocean Atlas 2013 (Locarnini et al., 2013; Zweng et al., 2013). SD designates the standard deviation of the WOA13 data.

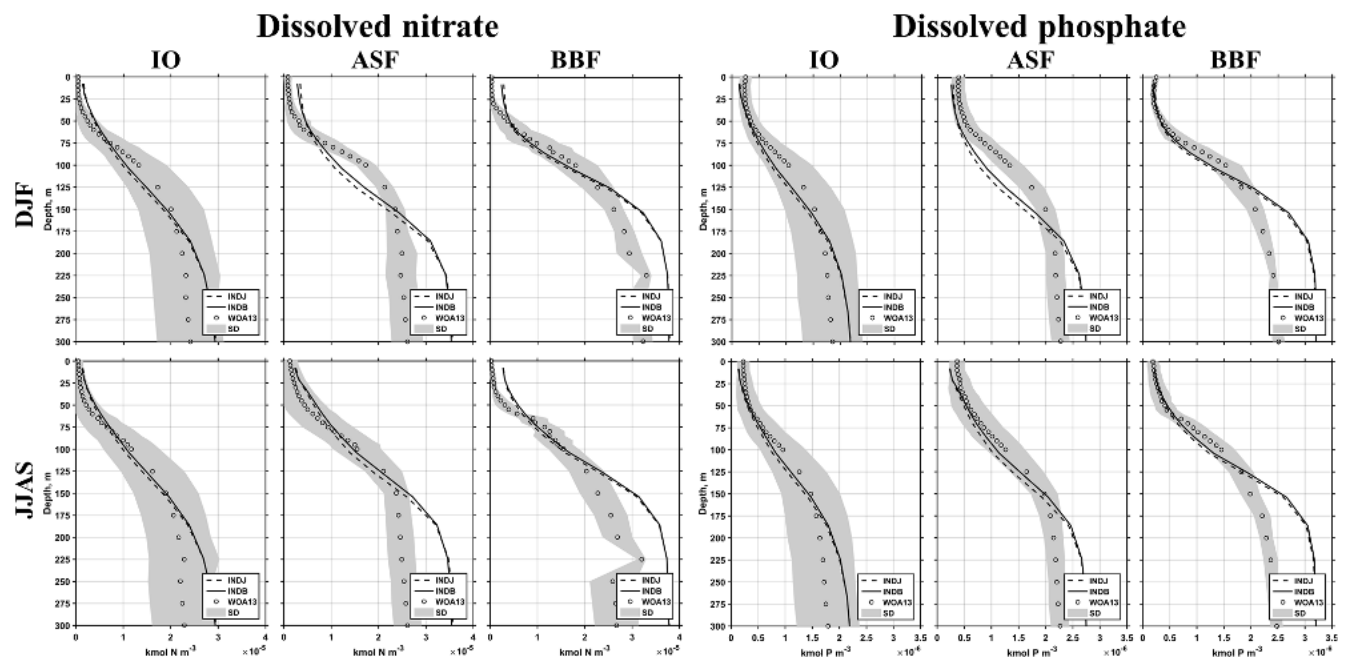


Figure 7. Vertical profiles of dissolved nitrate and phosphate time-averaged seasonally (DJF, JJAS) for the period 1975–2004. INDJ and INDB designate the model runs. WOA13 designates the climatic data from the World Ocean Atlas 2013 (Garcia et al., 2014). SD designates the standard deviation of the WOA13 data.

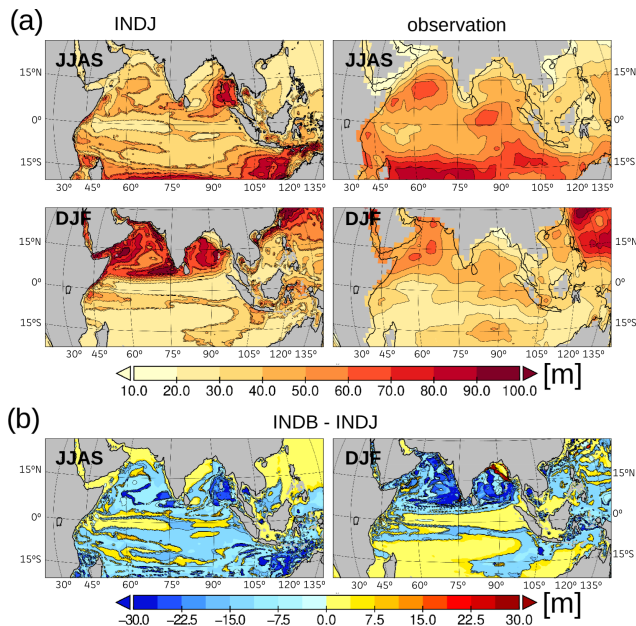


Figure 8. (a) Upper panel: monsoon season (JJAS) mixed-layer depth as calculated in the INDJ experiment (left) and from observational data (de Boyer Montégut et al., 2004; right). Lower panel: same as upper panel but for the winter season (DJF). (b) Mixed-layer depth difference between two model simulations (INDB–INDJ) for monsoon (left) and winter (right) seasons. All fields are time-averaged seasonally (DJF, JJAS) for the period 1975–2004.

both simulations the extension of this area is larger than in WOA data sets. In the Bay of Bengal, the model simulates a clear east–west gradient with a deeper thermocline in the east compared to the west. Such a pattern is also observed in WOA to some extent. To the south of the Equator the thermocline shoals in an extended zonal band with depths well below 50 m. This is likewise seen in WOA, though this is less pronounced there. During the winter monsoon, the very shallow thermocline in the coastal Arabian Sea strongly deepens in response to changed monsoon (Fig. 13a). This seasonal change is more pronounced in the model simulations but is still significant in the WOA data sets. This indicates that the seasonal variability is well represented in the model near the coasts.

The simulated thermocline depth is almost everywhere shallower when including the fully coupled biogeochemical variability in the parameterization of SWR attenuation in the water (Fig. 13b) in both monsoon and winter seasons. The explicit use of phytoplankton in the radiated heat transfer (INDB experiment) leads to more heat absorption in the upper layers and less heat absorption in lower layers. As a result, the thermocline shifts upward compared to the Jerlov type absorption (INDJ experiment), which follows a simple exponential curve with a constant exponent.

3.2 Atmosphere

Here we study the regional distribution of some key atmospheric fields over the South Asia CORDEX region and validate them for winter (DJF) and monsoon (JJAS) seasons over the 1975–2004 period. In Sect. 3.2.1 we focus on the regional distribution of 2 m air temperature (T2M) biases relative to the ERA5 reanalysis (Copernicus Climate Change Service, 2020). Also, temperature differences between the INDB and INDJ experiments are analyzed. This allows us to gain insight into temperature changes that occur in response to taking into account the variability of ocean biogeochemistry when calculating the SWR attenuation in the water. In Sect. 3.2.2 the same procedure is followed but taking into consideration the precipitation instead.

3.2.1 Air surface temperature

In both seasons, the mean surface temperature in ERA5 is clearly influenced by topography (Fig. 14a, d). In JJAS the cold bias over the Middle East and the warm bias over India (Fig. 14e) impact the strength and the path of the Findlater jet (Samson et al, 2017). The lowest values are reached on highly elevated terrain – especially in winter. The lowest temperatures are attained in world highest mountain ranges: the Himalaya, Pamir, Hindu Kush and the Tibetan Plateau. The highest monsoon season temperatures are reached along with the Indo river depression and the Arabian Peninsula. In experiment INDJ the winter daily mean temperatures are simulated quite well, and biases are relatively small (Fig. 14b and e); T2M is underestimated over most of the model domain, except for its northern and northwestern areas where positive biases can reach up to 5 °C. The negative biases are mostly below 2 °C, except for Tibet and Himalaya, where simulated T2M more than 4 °C colder than ERA5 can be found. The largest errors are found in depressed and/or highly elevated regions, and their values may be dependent on factors such as the limited number of meteorological stations in topographic highs and lows used for the assimilation in the region and the different representation of the orography in both REMO and ERA5. JJAS T2M biases are generally lower than in winter, with a similar dependence on orography. They become positive over most of the Indian subcontinent with maximum values over the northern Indo river basin where mean temperatures are up to 4 °C above ERA5. Over the ocean, a positive bias develops in the region where the monsoon winds are stronger. In general, the most considerable T2M biases are located in regions where larger temperatures are obtained, pointing to a role of the simulated nocturnal boundary layer and/or radiative fluxes. As shown in Samson et al. (2017), radiative fluxes (as well as winds and precipitation) are influenced by the representation of the land surface albedo, and this influence is important in this region. Like for the SST, ocean biogeochemical feedback variability leads to a colder surface air temperature over most of the ocean. In DJF the

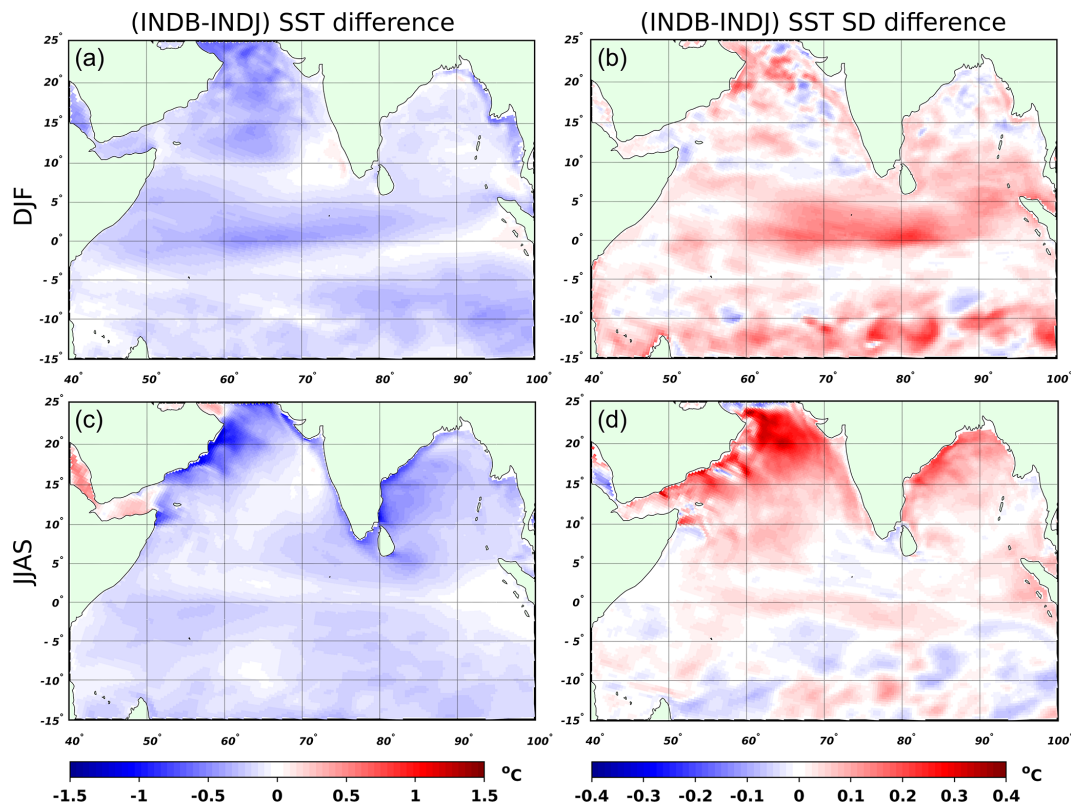


Figure 9. Spatial distribution of the difference between model runs (INDB–INDJ) for SST (a, c) and SST standard deviation (SD, b, d). SST and its standard deviation are time-averaged seasonally (DJF, JJAS) for the period 1975–2004.

cooling is stronger over the Arabian Sea and the equatorial strip, reinforcing the weak negative biases already present in INDJ. Over the land, taking into account the marine biogeochemical variability in INDB slightly improves the cold bias in northwestern and southern India. Still, it leads to a cooling in the central part. The ocean cooling in INDB is also present in JJAS, with stronger values near the western coast of the Arabian Sea and the Bay of Bengal, downstream of the monsoon winds.

3.2.2 Monsoon precipitation

The monsoon season in South Asia is shaped by different processes which change the atmospheric circulation due to the monsoon season strengthening of the ocean–land temperature contrast. The spatial structure of the observed monsoon precipitation is characterized by two regions of strong rainfall over land (Fig. 15a). The first is located windward, over the western coast of India, Myanmar and the southern side of the Himalayas. The second region which covers Bangladesh, central India and the eastern coast of the Indian peninsula is the area of maximum monsoon precipitation over the land. The precipitation is weaker over the northwest of India and Pakistan (Kumar et al., 2013). The intricate orography and physical mechanisms involved make the simulation of the

monsoon precipitation a difficult task both for global and regional models (Lucas-Picher et al., 2011). However, stand-alone simulations with REMO have been shown to be able to reproduce spatial monsoon precipitation patterns rather well, although a better quantitative agreement is desirable (Kumar et al., 2014). For instance, the precipitation over south and central India is overestimated, while the precipitation over the Indo-Ganges plain is strongly underestimated. A wet bias is usually found over the Bay of Bengal and the southern Indian Ocean.

As shown in previous versions of the model (Kumar et al., 2014; Paxian et al., 2016), ROM is able to improve the performance of REMO, simulating more realistic precipitation. The coupling reduces the magnitude of the biases, especially in the regions where REMO has the most substantial biases, near the eastern coasts of the Arabian Sea and the Bay of Bengal (Fig. 15b). It should be noted that in both INDJ and INDB experiments ROM is forced by MPI-ESM and the atmospheric biases of the driving ESM influence the results (e.g., Cabos et al., 2020).

Besides the total precipitation, in Fig. 15d–e we show the convective (thereafter APRC) and in Fig. 15g–h the large-scale (thereafter APRL) component of the precipitation. We can see that in INDJ the main contribution to the biases over the ocean near the eastern coast of the Arabian Sea comes

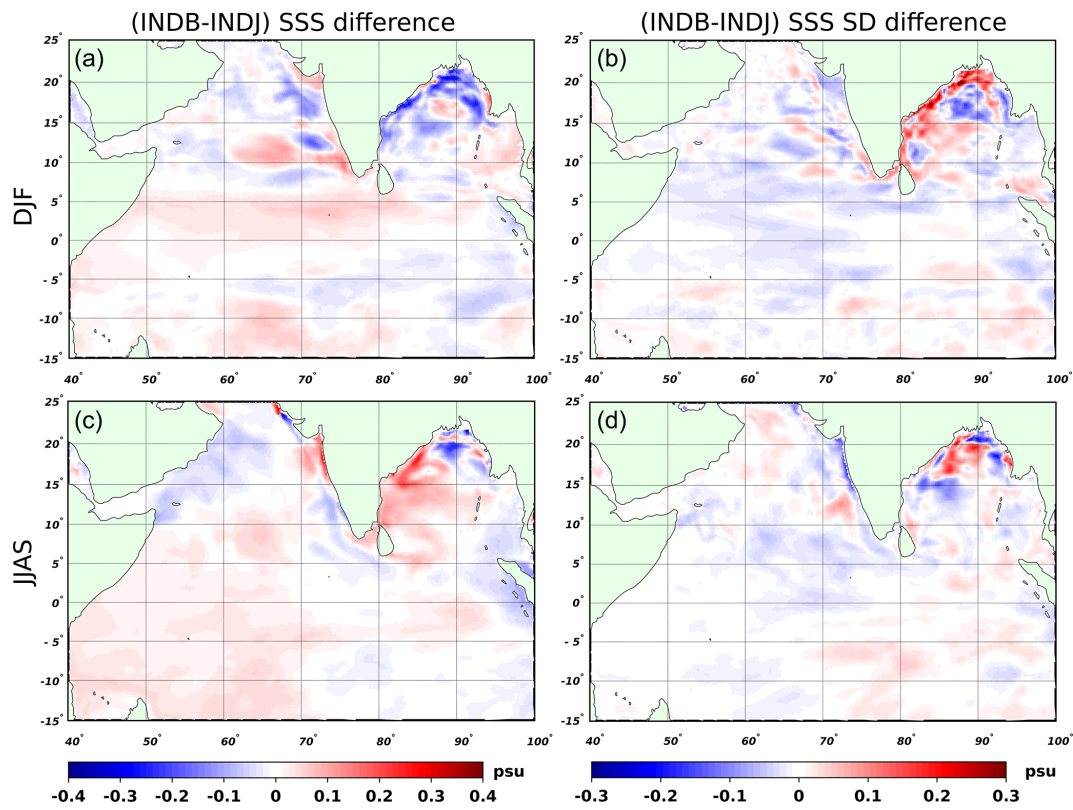


Figure 10. Spatial distribution of the difference between model runs (INDB–INDJ) for SSS (a, c) and SSS standard deviation (SD, b, d). SSS and its standard deviation are time-averaged seasonally (DJF, JJAS) for the period 1975–2004.

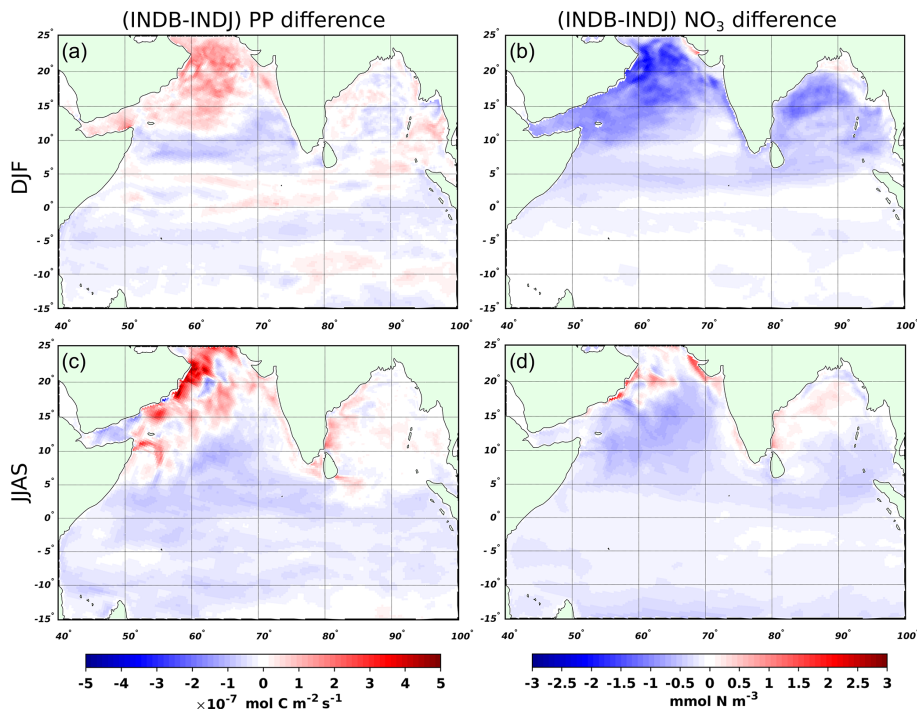


Figure 11. Spatial distribution of the difference between the model runs (INDB–INDJ) for PP (a, c) and NO₃ (b, d). PP and NO₃ are time-averaged seasonally (DJF, JJAS) for the period 1975–2004.

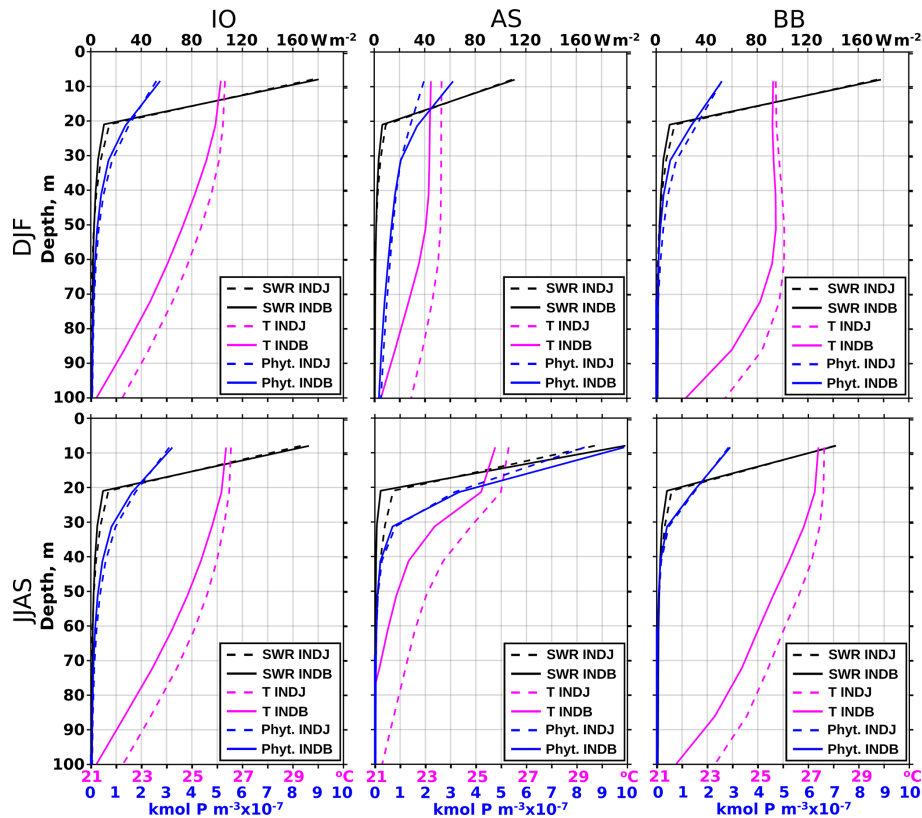


Figure 12. Vertical profiles of shortwave radiation (SWR), water temperature (T) and phytoplankton concentration (Phyt) in the INDJ and INDB experiments.

from APRC, while over the coastal land the main contributor is APRL. The opposite is true for the eastern coast of the Bay of Bengal, especially in Myanmar where the main contributor over the ocean and the coastal regions is APRL, with a lesser contribution from APRC. To the south of the Equator, between 10° S and the Equator, both components give a contribution of similar magnitude, albeit the large-scale component is stronger. Here, both components show a similar displacement of the region of maximum precipitation to the south. While the magnitude of the convective precipitation is lower than in ERA5, the large-scale component is stronger and more zonal than the ERA5 large-scale precipitation.

In the INDB experiment, taking into account the variability of marine biogeochemistry when calculating SWR penetration into the water leads to drying over most of the ocean, especially over the Bay of Bengal, central and northeastern the Arabian Sea, and the strip south of the Equator. An apparent reduction in precipitation can also be found inland, along the western Indian coast. As seen in Fig. 15f and i, the contribution of convective and large-scale components to these differences vary along the regions.

In the INDB experiment, APRC gives the main contribution (in terms of precipitation) over the Bay of Bengal, the central part of the Arabian Sea and the coastal regions of western India. APRL gives the main contribution to the dry-

ing in northern–central India, while in Myanmar it causes a wetting, thus offsetting the impact on APRC. To the south of the Equator, between 10° S and 0° , the impact is similar to both precipitation components.

4 Discussion

The effect of the spatial and temporal variability of a fully coupled marine ecosystem upon SWR attenuation in water (experiment INDB) leads to a cooling of the ocean waters compared to a reference INDJ experiment where a constant attenuation coefficient was set equal to 0.06 m^{-1} (Jerlov IB water type). Generally, taking into account the phytoplankton when calculating light extinction in the ocean leads to a warming of the upper ocean layer and cooling of subsurface layers compared to a “no-bio” reference experiment (e.g., Nakamoto et al., 2000; Lengaigne et al., 2007; Park et al., 2014a, b; Park and Kug, 2014). But, as emphasized in Lengaigne et al. (2007), the sign of the effect is determined by the choice of the reference experiment. If a truly “no-bio” approach is implemented in a reference experiment (a “dead ocean” case), then the SST in the experiments where either a constant chlorophyll a concentration or fully cou-

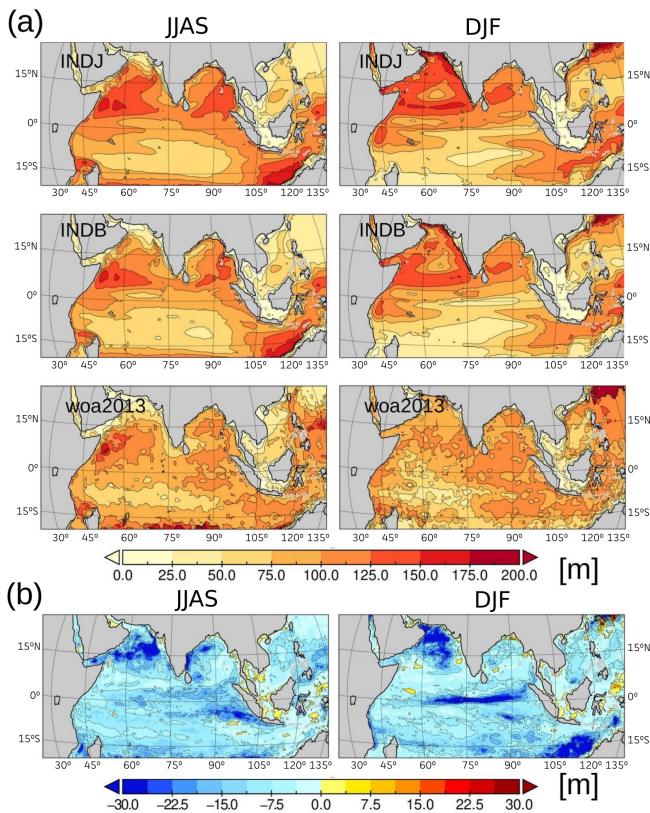


Figure 13. (a) Comparison of simulated thermocline depth with thermocline depth derived from WOA 2013 data sets for JJAS (left) and DJF (right). (b) The difference in thermocline depth between the two runs (INDB–INDJ) for JJAS (left) and DJF (right).

pled biogeochemical model is implemented becomes higher compared to the reference experiment.

Our results show that in INDB the SST and subsurface waters are cooler than in INDJ over most of the model domain. The attenuation coefficient used in INDJ (0.06 m^{-1}) is not equal to a freshwater attenuation coefficient (0.03 m^{-1}) (e.g., Ilyina et al., 2013). In fact, an attenuation coefficient constant in space and time of 0.06 m^{-1} used in the INDJ experiment corresponds to oceanic water masses with relatively small amounts of phytoplankton. Still, it would be incorrect to say that SWR absorption in such waters is fully controlled only by fresh water. It means that in the INDJ experiment the ocean absorbs the incoming SWR more actively than if we use the attenuation coefficient equal to 0.03 m^{-1} . This detail is crucial to explaining why the water temperature is cooler in the INDB experiment compared to INDJ. The reason for that is the parameterization used for the SWR extinction in INDB. As given in Gröger et al. (2013), the attenuation coefficient in this parameterization depends on a constant part representing water attenuation (0.03 m^{-1}) and a variable part representing the attenuation by phytoplankton (for details see Appendix A in Gröger et al., 2013). Thus, if phytoplankton concentration is low then the final magnitude of the attenuation coefficient

in INDB may be smaller than 0.06 m^{-1} . Analysis of the annual-mean and seasonal-mean phytoplankton distribution in the northern part of the Indian Ocean in both experiments and in satellite data (e.g., Fig. 3 herein or Fig. 2 in Liu et al., 2013) has revealed that this is almost always the case – the observed phytoplankton concentrations in the study area are not enough to raise the attenuation coefficient in the INDB experiment up to an exact value of 0.06 m^{-1} or higher in the domains considered in our analysis (IO, ASF, BBF, etc). Indeed, Fig. 16 demonstrates the spatial distribution of the calculated attenuation coefficient at the ocean surface averaged annually (ANN) and seasonally (DJF, MAM, JJAS, ON) in the INDB experiment, as well as attenuation coefficient obtained by SeaWiFS measurements (NASA Goddard Space Flight Center, 2021c) and averaged in the same way.

The climatic annual-mean value of the attenuation coefficient in the INDB experiment (0.056 m^{-1}) is closer to that in SeaWiFS data (0.051 m^{-1}) than the INDJ's value (0.06 m^{-1}). Compared to the fixed attenuation coefficient used in the INDJ experiment, in the INDB experiment the attenuation coefficient has its temporal and spatial variability which roughly replicate that of SeaWiFS, except for the winter period (DJF), taking into account the known uncertainty in the determination of this characteristic. The SeaWiFS's minimum coefficient value occurs in the pre-monsoon season (MAM, 0.042 m^{-1}) and maximum occurs in the monsoon season (JJAS, 0.059 m^{-1}). It corresponds to model results: the minimum occurs in the pre-monsoon season (MAM, 0.053 m^{-1}) and maximum is in monsoon season (JJAS, 0.059 m^{-1}). Such seasonal variability allows us to examine the influence of marine biogeochemical variability upon the climatic characteristics in the current study.

Figure 12 clearly demonstrates that for the upper 100 m layer the water temperature differences between INDB and INDJ experiments in the surface layers are less than the differences between them in the deeper layers. Consideration of further changes in this difference with increasing depth showed that the maximum difference occurs at depths of about 100 m or less and in layers lying below the depth of the maximum difference, it decreases to negligible values at depths of 180–240 m. It means that the SWR absorption and vertical water temperature distribution in the INDB experiment follows the same mechanism as reported in other above-mentioned studies – warming of the surface layer due to additional SWR absorption by phytoplankton and cooling of the subsurface waters, compared to experiment with constant attenuation coefficient. But in our study, we compare INDB results not with a reference experiment with an attenuation coefficient of 0.03 m^{-1} (without phytoplankton), but with a more realistic experiment with an attenuation coefficient equal to 0.06 m^{-1} (INDJ). The reason for such a choice is that we study not the marine biogeochemical input as it is, but the impact of its variability upon regional climate. That is why for the basic model run in this study we chose the SWR attenuation scheme with constant attenuation coefficient.

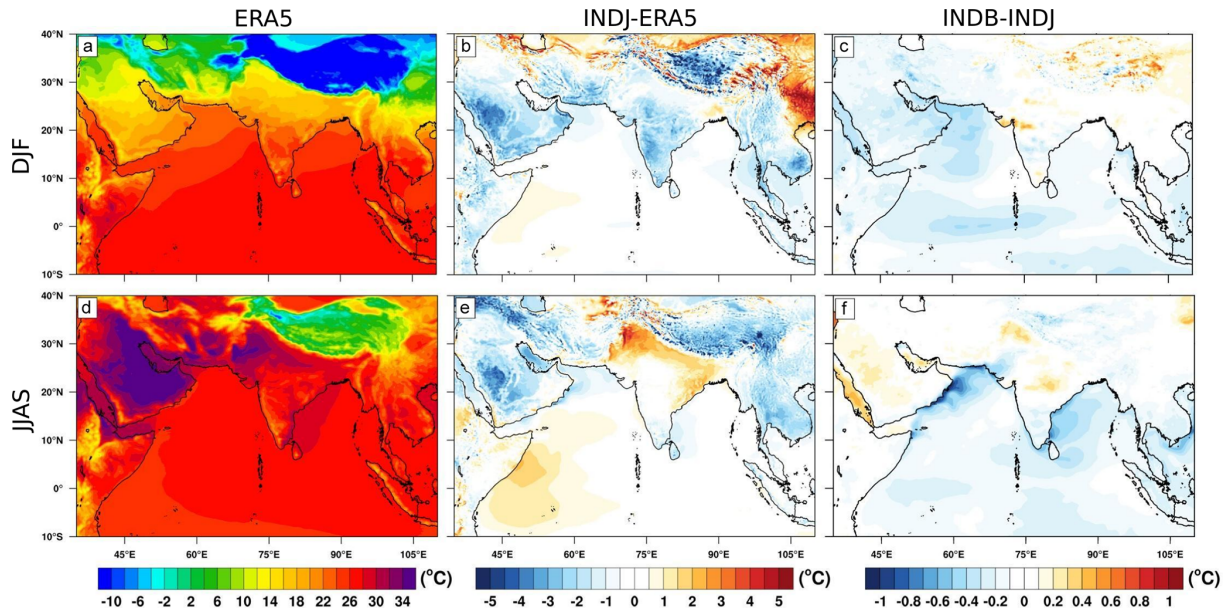


Figure 14. DJF (upper row) and JJAS (lower row). (a, d) 2 m temperature ERA5 climatology. (b, e) Bias for the experiment INDJ; (c, f) INDB–INDJ difference.

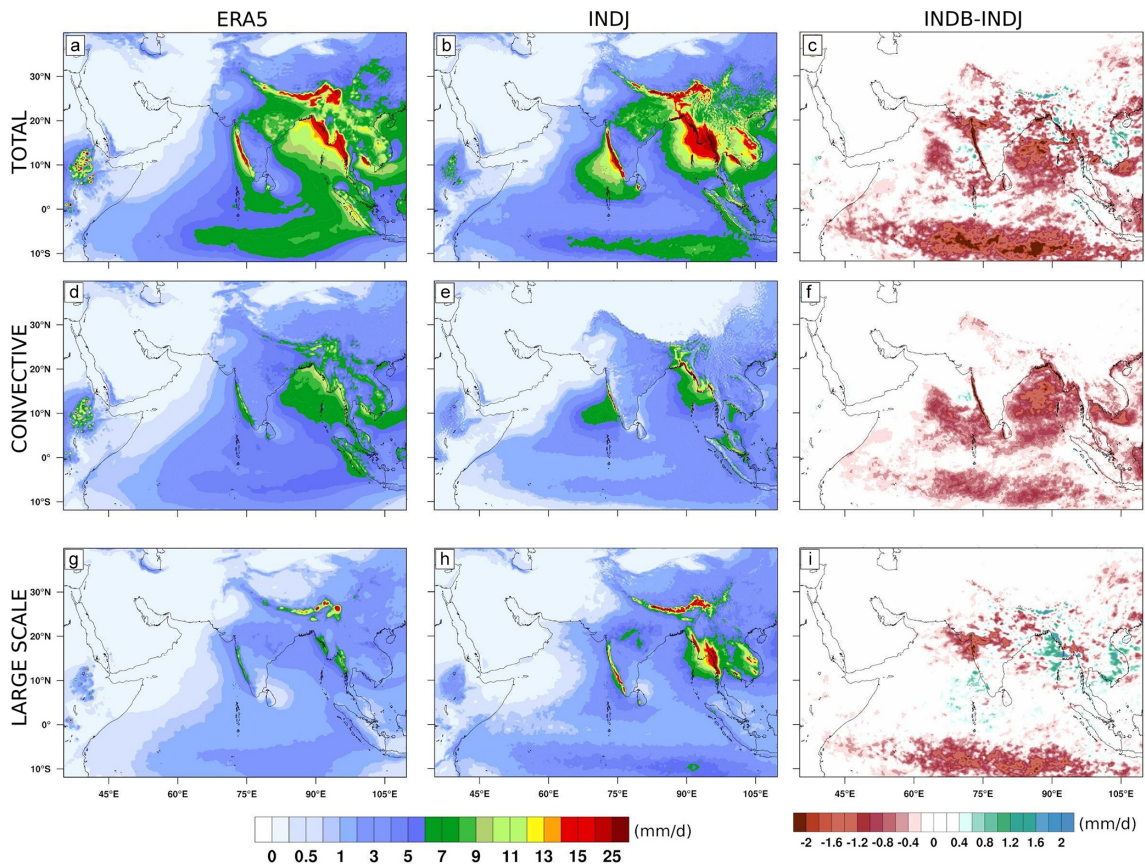


Figure 15. JJAS precipitation for ERA5 (a, d, g), INDJ experiment (b, e, h), and the differences between INDB and INDJ (c, f, i) for total precipitation (a–c), convective precipitation (d–f) and large-scale precipitation (g–i).

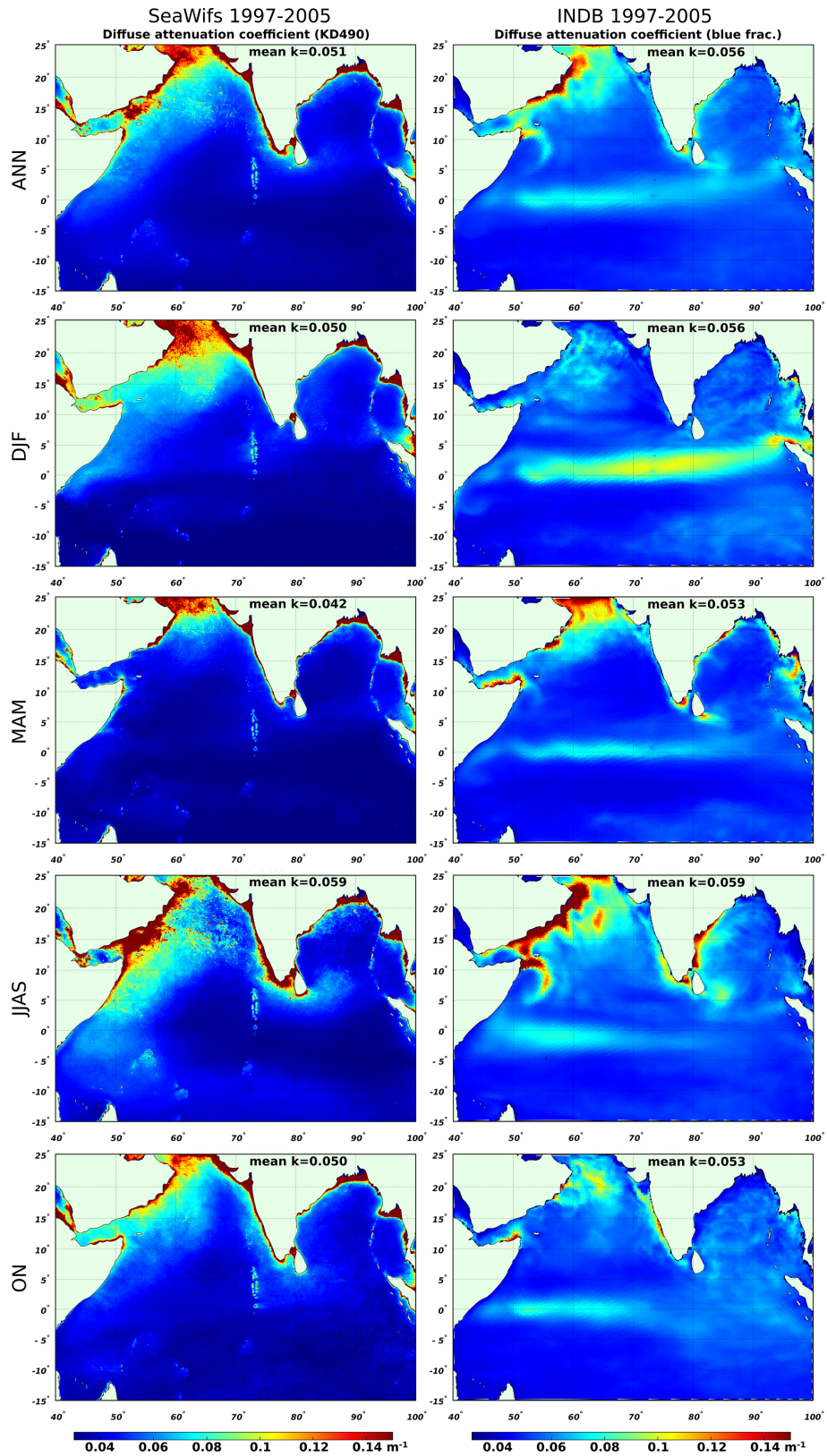


Figure 16. Spatial distribution of the attenuation coefficient at the ocean surface averaged annually (ANN) and seasonally (DJF, MAM, JJAS, ON). Left column – SeaWiFS data (NASA Goddard Space Flight Center, 2021c) averaged over 1997–2005; right column – INDB results averaged over 1997–2005. For all figures, a mean value of the attenuation coefficient (inside the domain) is presented.

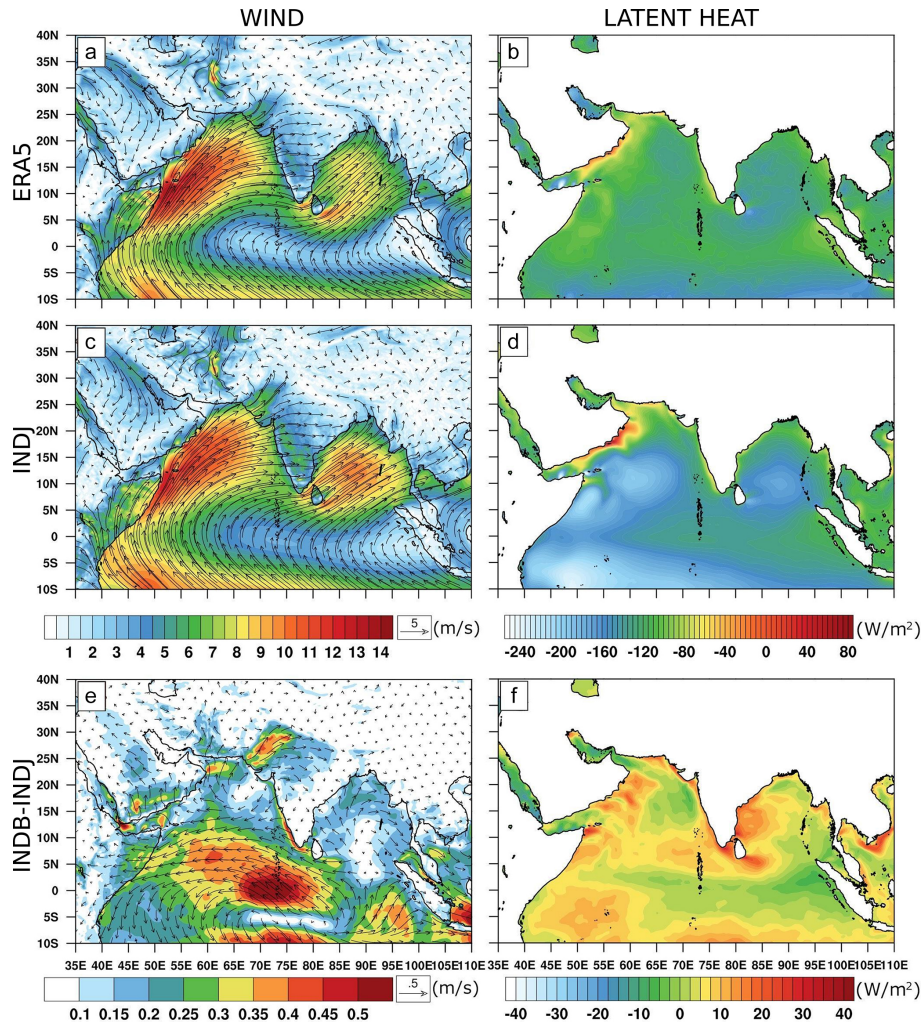


Figure 17. JJAS wind (a, c and e, arrows are wind velocities, the color scale is the wind speed module) and latent heat (b, d and f, the color scale is the latent heat flux) for ERA5 (a, b); INDJ experiment (c, d) and (INDB–INDJ) difference (e, f).

Under the changing climate conditions, the variability of marine biogeochemistry and its corresponding influence on the SWR absorption by the ocean may be an important factor in climate simulations. Thus, the investigation of the differences between the INDJ and INDB experiments presented in this paper is focused on this specific problem. In this respect, making model simulations with fully absent phytoplankton impact on the light absorption while studying regional climate would not make much sense because such a situation is unrealistic. Using the light attenuation parameterization of the INDB experiment but with fully absent phytoplankton would mean neglecting biology completely. However, such additional experiments would help to quantify the effect of phytoplankton in our RESM configuration. Still, taking into account previous studies focused on this matter, significant demands of the presented fully coupled RESM and limited computational resources, we are compelled to constrain ourselves on the potential research directions in this paper.

Regarding the value of the attenuation coefficient in the reference INDJ experiment equal to 0.06 m^{-1} , such a choice was dictated by the following main reasons. Firstly, in a lot of previous studies with the ROM modeling system the reference attenuation coefficient equal to 0.06 m^{-1} was used (e.g., Sein et al., 2020; Tangang et al., 2020; Zhu et al., 2020; Cabos et al., 2017, 2019; Paeth et al., 2017; Paxian et al., 2016; Paulsen et al., 2018). The choice of this attenuation coefficient was justified by correctly modeled global primary production, better representation of the ITCZ and heat budget, which were in a good agreement with observations. Since the ocean component of the ROM modeling system is global, we have to use globally adjusted model's parameters in the present study as well. Secondly, the choice of the attenuation coefficient in INDJ equal to 0.06 m^{-1} does not assume an unrealistically green ocean. As we have already shown (Fig. 16), the SeaWiFS satellite measurements give seasonal climatological values of the attenuation coef-

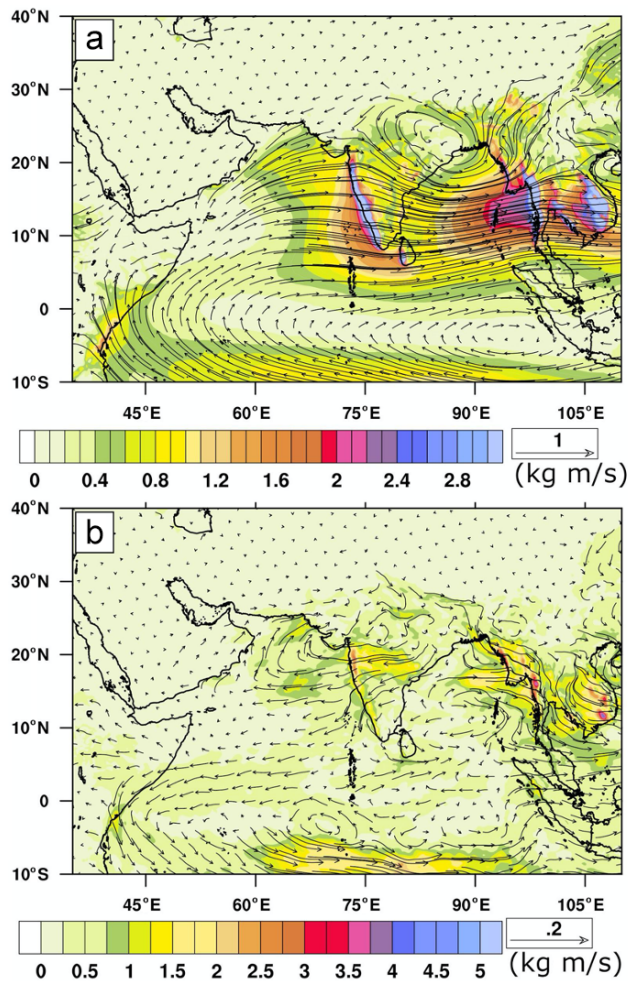


Figure 18. JJAS horizontal transport of cloud water (arrows show the vector of cloud water transport, the color scale is its module) in INDJ (a) and INDB–INDJ difference (b).

cient equal to $0.044\text{--}0.063\text{ m}^{-1}$ for the considered domain, with the annual-mean climatic value of 0.052 m^{-1} . Finally, Rochford et al. (2001) reported the assessment of global attenuation coefficient distribution in the World Ocean based on satellite data. Following their results, the value 0.06 m^{-1} can be seen as a good estimate of background attenuation coefficient for our domain, except the very coastal waters and Arabian Sea in August (for details, see Plate 1 and 2 in their paper at the page no. 30926).

Thus, a correctly adjusted constant light attenuation coefficient can ensure correct global-mean estimates of primary production, heat budget, etc. Still, it may under- or overestimate SWR attenuation regionally. In this way of thinking, the use of a completely different parameterization of light attenuation, as is implemented in INDB in this study, is seen as a good approach for a global model to take into account regional features because it includes a spatially and temporally varying phytoplankton-dependent attenuation coefficient.

In the INDB experiment, the thermocline shifts upward compared to the INDJ run where a simple exponential curve of light attenuation is implemented. This is due to a sharper vertical gradient of water temperature in INDB (Fig. 12) induced by the non-homogeneity of the vertical distribution of phytoplankton. Hence, in the INDB experiment we see increased light absorption in the upper ocean layers and decreased – in the subsurface layers, compared to INDJ where a constant attenuation coefficient controls the SWR absorption.

The different light attenuation parameterization implemented in INDB has cascading effects on model physics, like altered SST, which further translates into altered atmosphere dynamics. Due to the temporarily varying chlorophyll *a* concentrations in the ocean surface layer and subsequent variable heat absorption, SSTs are by far more variable in the INDB experiment than in INDJ (Fig. 9).

The higher phytoplankton primary production in INDB (Fig. 11) is most likely the effect of the decreased mixed-layer depth which allows phytoplankton to prevail longer in the euphotic layer. This effect is more pronounced to the north of 10° N where the thermocline is relatively deep (and a reduction of the mixed-layer depth in INDB is most effective). In regions where the thermocline is generally shallower (to the south of 10° N) this effect is of minor importance as light is less limiting there.

During JJAS, the simulated wind in INDJ is slightly weaker than in ERA5 in the Arabian Sea but stronger in the Bay of Bengal (compare Fig. 17a and c). In the latter, stronger winds lead to stronger latent heat fluxes, while the opposite is true for the Arabian Sea where the weaker wind is associated with a stronger latent heat (Fig. 17b and d). This points to a different nature of the relationship between wind speed and latent heat in both regions, leading to stronger heat flux in both regions. The monsoon winds bring drier air into the Arabian Sea because it flows over colder water all the way from the equatorial region. Although the cold bias here leads also to a decrease in surface humidity, as the SST bias is lower, the surface humidity bias is lower. The resulting increase in the sea–air humidity difference overcomes the decrease in the wind, thus giving a stronger latent heat flux. This is not true for the west coast where most of the air comes from land (Wu et al., 2007). In the Bay of Bengal, the increase in latent heat is mainly associated with the simulated winds which are stronger than in ERA5. In the INDB experiment, the marine biogeochemical variability and corresponding variability of SWR absorption by the ocean causes a further cooling over the basin (Fig. 9), and this cooling causes a further drying over most of the domain, especially over the land in regions that are downstream of the monsoon winds. The drying is related to changes both in convection activity and moisture transport. Figure 18a shows the horizontal transport of cloud water for the INDJ experiment. This figure shows the contribution of the large-scale circulation to the monsoon rain. The Arabian Sea winds are

charged with moisture in their path to the Indian subcontinent and Sri Lanka, contributing to the large-scale precipitation in the eastern part of the basin and the coastal regions (Fig. 15h). The wind, which loses moisture over the land, is again recharged over the Bay of Bengal, contributing to the strong precipitation in the eastern part of the Bay of Bengal, Myanmar and southeastern Asia. It is worth noting the recirculation of cloud water in northeastern India due to the presence of the Himalayan range, which influences the amount of precipitation there. The marine biogeochemical variability and corresponding change of SWR absorption affects the precipitation over the Arabian Sea and the Bay of Bengal in different ways. From one side, it reduces the transport of humidity across the Equator towards the eastern part of the basin, reducing the large-scale precipitation there and in the adjacent coastal regions, reinforcing the effect of the colder water on the convective precipitation. In the Bay of Bengal, it reinforces the transport of humidity, increasing the large-scale precipitation, contouring the decrease in convective precipitation due to the SST cooling (Fig. 18b).

5 Conclusions

A regional Earth system model based on the ROM model (Sein et al., 2015) has been implemented for the CORDEX South Asia region. We use the model to investigate the effect of taking into account the full spatial and temporal variability of the marine ecosystem while calculating light absorption by water upon the regional climate. Two model simulations are conducted using CMIP5 historical forcing for the period 1920–2005. They differ only by ocean SWR attenuation parameterizations.

The effect of the spatial and temporal variability of a fully coupled marine ecosystem upon SWR attenuation in water (experiment INDB) leads to a water temperature decline in the ocean compared to a reference INDJ experiment where a constant light attenuation coefficient was set equal to 0.06 m^{-1} (Jerlov IB water type). Based on the analysis of the annual-mean and seasonal-mean phytoplankton distribution in the northern part of the Indian Ocean attenuation in both experiments and in satellite data, we can conclude that the reason for this is the low spatially averaged phytoplankton concentrations in the analyzed areas; i.e., concentrations are not enough to raise the attenuation coefficient in INDB (which depends on chlorophyll *a* concentration) up to 0.06 m^{-1} as used in a reference experiment (INDJ). However, the strength (and direction) of temperature alteration strongly relates to the Jerlov type chosen for the reference simulation, in agreement with earlier findings (e.g., Lengaigne et al., 2007).

Both simulations adequately reproduced the precipitation climatology for all seasons. In particular, the spatial pattern of the monsoon precipitation is well simulated, albeit with some systematic wet biases which are more assertive over

the eastern parts of the Arabian Sea and the Bay of Bengal and the adjacent coastal regions. We found that the marine biogeochemical variability in INDB and the corresponding change of SWR absorption also affects the amount of precipitation in the model, leading to drying over most of the basin in the monsoon season. The associated SST cooling leads in general to a reduction of the precipitation but affects in different ways the two components of the precipitation. In the Arabian Sea the reduction of the transport of humidity across the Equator leads to a reduction of the large-scale precipitation in the eastern part of the basin, reinforcing reduction of the convective precipitation. In the Bay of Bengal it increases the large-scale precipitation, contouring the decrease in convective precipitation due to the SST cooling.

Thus, in comparison with simulation using a constant light attenuation coefficient (0.06 m^{-1} , Jerlov IB water type), the major impacts of including the full biogeochemical coupling with corresponding light attenuation in water, which in turn depends on variable chlorophyll *a* concentration, include the enhanced phytoplankton primary production, a shallower thermocline, decreased SST and water temperature in subsurface layers, with cascading effects upon the model ocean physics which further translates into altered atmosphere dynamics.

In summary, the presented model demonstrates the locally substantial impact of phytoplankton-related chlorophyll on the atmospheric climate of the Indian Ocean. However, this study does not take into account the direct impact of biology (i.e., productivity) on atmospheric $p\text{CO}_2$ and the subsequent impact on the atmospheric radiation budget. Because of this, the impact of marine biology on climate may be underestimated.

Code availability. The model code is available by request.

Data availability. The data sets generated during and/or analyzed during the current study are available from the corresponding author upon reasonable request.

Author contributions. DVS and VAR formulated the concept of the paper and participated in its writing. AYD, SDM, WC, PK and MG carried out the analysis of simulated data. DVS did the model runs. DJ participated in supervising and provided computational resources. SDM, WC, AYD and MG wrote the original draft. All the co-authors participated in reviewing and editing the draft version of the manuscript.

Competing interests. The contact author has declared that neither they nor their co-authors have any competing interests.

Disclaimer. Publisher's note: Copernicus Publications remains neutral with regard to jurisdictional claims in published maps and institutional affiliations.

Acknowledgements. This work is jointly funded by Russian Science Foundation (RSF), Russia (project 19-47-02015), and Department of Science and Technology (DST), Government of India (grant no. DST/INT/RUS/RSF/P-33/G), through a project "Impact of climate change on South Asia extremes: A high-resolution regional Earth System Model assessment". The research was performed in the framework of the state assignment of the Ministry of Science and Higher Education of Russia (no. 0128-2021-0014). This work used resources of the Deutsches Klimarechenzentrum (DKRZ) granted by its Scientific Steering Committee (WLA) under project ID ba1144. We thank the anonymous reviewers and Andreas Oschlies for the constructive suggestions and critical remarks, which helped to improve the paper.

Financial support. This research has been supported by the Russian Science Foundation (grant no. 19-47-02015, 1 January 2019 until 31 December 2021).

The article processing charges for this open-access publication were covered by the Alfred Wegener Institute, Helmholtz Centre for Polar and Marine Research (AWI).

Review statement. This paper was edited by Roland Séférian and reviewed by two anonymous referees.

References

- Anderson, T. R., Ryabchenko, V. A., Fasham, M. J. R., and Gorchakov, V. A.: Denitrification in the Arabian Sea: A 3D ecosystem modelling study, *Deep-Sea Res.* Pt. I, 54, 2082–2119, <https://doi.org/10.1016/j.dsr.2007.09.005>, 2007.
- Boyer, T. P., Garcia, H. E., Locarnini, R. A., Zweng, M. M., Mishonov, A. V., Reagan, J. R., Weathers, K. A., Baranova, O. K., Seidov, D., and Smolyar, I. V.: World Ocean Atlas 2018, NOAA NCEI [data set], <https://accession.nodc.noaa.gov/NCEI-WOA18> (last access: 30 November 2021), 2018.
- Cabos, W., Sein, D. V., Pinto, J. G., Fink, A. H., Koldunov, N. V., Alvarez, F., Izquierdo, A., Keenlyside, N., and Jacob, D.: The South Atlantic Anticyclone as a key player for the representation of the tropical Atlantic climate in coupled climate models, *Clim. Dynam.*, 48, 4051–4069, <https://doi.org/10.1007/s00382-016-3319-9>, 2017.
- Cabos, W., Sein, D. V., Durán-Quesada, A., Liguori, G., Koldunov, N. V., Martínez-López, B., Alvarez, F., Sieck, K., Limareva, N., and Pinto, J. G.: Dynamical downscaling of historical climate over CORDEX Central America domain with a regionally coupled atmosphere–ocean model, *Clim. Dynam.*, 52, 4305–4328, <https://doi.org/10.1007/s00382-018-4381-2>, 2019.
- Cabos, W., de la Vara, A., Álvarez-García, F. J., Sánchez, E., Sieck, K., Pérez-Sanz, J.-I., Limareva, N., and Sein, D. V.: Impact of ocean-atmosphere coupling on regional climate: the Iberian Peninsula case, *Clim. Dynam.*, 54, 4441–4467, <https://doi.org/10.1007/s00382-020-05238-x>, 2020.
- Choudhury, A. K. and Pal, R.: Phytoplankton and nutrient dynamics of shallow coastal stations at Bay of Bengal, Eastern Indian coast, *Aquat. Ecol.*, 44, 55–71, <https://doi.org/10.1007/s10452-009-9252-9>, 2010.
- Copernicus Climate Change Service: ERA5: Fifth generation of ECMWF atmospheric reanalyses of the global climate, CDS, <https://cds.climate.copernicus.eu/cdsapp#!/home>, last access: 1 July 2021.
- D'Asaro, E., Altabet, M., Kumar, N. S., and Ravichandran, M.: Structure of the Bay of Bengal oxygen deficient zone, *Deep-Sea Res.* Pt. II, 179, 104650, <https://doi.org/10.1016/j.dsr.2019.104650>, 2020.
- De, T. K., De, M., Das, S., Chowdhury, C., Ray, R., and Jana, T. K.: Phytoplankton abundance in relation to cultural eutrophication at the land-ocean boundary of Sunderbans, NE Coast of Bay of Bengal, India, *J. Environ. Stud. Sci.*, 1, 169, <https://doi.org/10.1007/s13412-021-00695-0>, 2011.
- De Boyer Montégut, C., Madec, G., Fischer, A. S., Lazar, A., and Iudicone, D.: Mixed layer depth over the global ocean: An examination of profile data and a profile-based climatology, *J. Geophys. Res.*, 109, C12003, <https://doi.org/10.1029/2004JC002378>, 2004.
- Fu, W., Randerson, J. T., and Moore, J. K.: Climate change impacts on net primary production (NPP) and export production (EP) regulated by increasing stratification and phytoplankton community structure in the CMIP5 models, *Biogeosciences*, 13, 5151–5170, <https://doi.org/10.5194/bg-13-5151-2016>, 2016.
- Garcia, H. E., Locarnini, R. A., Boyer, T. P., Antonov, J. I., Baranova, O. K., Zweng, M. M., Reagan, J. R., and Johnson, D. R.: World Ocean Atlas 2013, Volume 4: Dissolved Inorganic Nutrients (phosphate, nitrate, silicate), edited by: Levitus, S. and Mishonov, A., NOAA Atlas NESDIS, 25 pp., 2014.
- Giorgi, F.: Regional climate modeling: status and perspectives, *J. Phys.* IV France, 139, 101–118, <https://doi.org/10.1051/jp4:2006139008>, 2006.
- Gröger, M., Maier-Reimer, E., Mikolajewicz, U., Moll, A., and Sein, D.: NW European shelf under climate warming: implications for open ocean – shelf exchange, primary production, and carbon absorption, *Biogeosciences*, 10, 3767–3792, <https://doi.org/10.5194/bg-10-3767-2013>, 2013.
- Gröger, M., Dieterich, C., Meier, M., and Schimanke, S.: Thermal air-sea coupling in hindcast simulations for the North Sea and Baltic Sea on the NW European shelf, *Tellus A.*, 67, 26911, <https://doi.org/10.3402/tellusa.v67.26911>, 2015.
- Hagemann, S. and Dumenil, L.: A parameterization of the lateral waterflow for the global scale, *Clim. Dynam.*, 14, 17–31, 1998.
- Ilyina, T., Six, K. D., Segsneider, J., Maier-Reimer, E., Li, H., and Núñez-Riboni, I. X.: Global ocean biogeochemistry model HAMOCC: Model architecture and performance as component of the MPI-Earth system model in different CMIP5 experimental realizations, *J. Adv. Model. Earth Syst.*, 5, 287–315, <https://doi.org/10.1029/2012MS000178>, 2013.
- IPCC: Climate Change 2014: Synthesis Report. Contribution of Working Groups I, II and III to the Fifth Assessment Report of the Intergovernmental Panel on Climate Change, IPCC, Geneva, Switzerland, 151 pp., 2014.

- Jacob, D.: A note to the simulation of the annual and interannual variability of the water budget over the Baltic Sea drainage basin, *Meteorol. Atmos. Phys.*, 77, 61–73, 2001.
- Jacob, D., Hurk, B., Andrae, U., Elgered, G., Fortelius, C., Graham, L., Jackson, S., Karstens, U., Köpken, C., Lindau, R., Podzun, R., Rockel, B., Rubel, F., Sass, B., Smith, R., and Yang, X.: A comprehensive model intercomparison study investigating the water budget during the BALTEX-PIDCAP period, *Meteorol. Atmos. Phys.*, 77, 19–43, 2001.
- Jerlov, N. G.: *Marine Optics*, Elsevier Oceanography Series, Elsevier, Amsterdam, The Netherlands, 230 pp., ISBN 9780080870502, 1976.
- Jungclaus, J. H., Fischer, N., Haak, H., Lohmann, K., Marotzke, J., Matei, D., Micolajewicz, U., Notz, D., and von Storch, J. S.: Characteristics of the ocean simulations in MPIOM, the ocean component of the MPI-Earth system model, *J. Adv. Model. Earth Syst.*, 5, 422–446, <https://doi.org/10.1002/jame.20023>, 2013.
- Kumar, P., Wiltshire, A., Mathison, C., Asharaf, S., Ahrens, B., Lucas-Picher, P., Christensen, J. H., Gobiet, A., Saeed, F., Hagemann, S., and Jacob, D.: Downscaled climate change projections with uncertainty assessment over India using a high resolution multi-model approach (Supplement), *Sci. Total Environ.*, 468–469, S18–S30, <https://doi.org/10.1016/j.scitotenv.2013.01.051>, 2013.
- Kumar, P., Sein, D., Cabos, W., and Jacob, D.: Improvement of simulated monsoon precipitation over South-Asia with a regionally coupled model ROM, in: 3rd International Lund Regional-Scale Climate Modelling Workshop 21st Century Challenges in Regional Climate Modelling: Workshop proceedings, edited by: Bärring, L., Reckermann, M., Rockel, B., and Rummukainen, M., Lund, Sweden, 16–19 June 2014, International Baltic Earth Secretariat Publications, Geesthacht, Germany, 434 pp., 2014.
- Lengaigne, M., Menkes, C., Aumont, O., Gorgues, T., Bopp, L., André, J.-M., and Madec, G.: Influence of the oceanic biology on the tropical Pacific climate in a coupled general circulation model, *Clim. Dynam.* 28, 503–516, <https://doi.org/10.1007/s00382-006-0200-2>, 2007.
- Levitus, S. B., Tim, P., Garcia, H. E., Locarnini, R. A., Zweng, M. M., Mishonov, A. V., Reagan, J. R., Antonov, J. I., Baranova, O. K., Biddle, M., Hamilton, M., Johnson, D. R., Paver, C. R., and Seidov, D.: World Ocean Atlas 2013 (NCEI Accession 0114815), NOAA NCEI [data set], <https://doi.org/10.7289/v5f769gt>, 2014.
- Liu, L., Feng, L., Yu, W., Wang, H., Liu, Y., and Sun, S.: The distribution and variability of simulated chlorophyll concentration over the tropical Indian Ocean from five CMIP5 models, *J. Ocean Univ. China*, 12, 253–259, <https://doi.org/10.1007/s11802-013-2168-y>, 2013.
- Locarnini, R. A., Mishonov, A. V., Antonov, J. I., Boyer, T. P., Garcia, H. E., Baranova, O. K., Zweng, M. M., Paver, C. R., Reagan, J. R., Johnson, D. R., Hamilton, M., and Seidov, D.: World Ocean Atlas 2013, Volume 1: Temperature, edited by: Levitus, S., and Mishonov, A., NOAA Atlas NESDIS, 40 pp., 2013.
- Lucas-Picher, P., Christensen, J. H., Saeed, F., Kumar, P., Asharaf, S., Ahrens, B., Wiltshire, A. J., Jacob, D., and Hagemann, S.: Can regional climate models represent the Indian monsoon?, *J. Hydrometeorol.*, 12, 849–868, <https://doi.org/10.1175/2011JHM1327.1>, 2011.
- Manizza, M., Le Quéré, C., Watson, A. J., and Buitenhuis, E. T.: Bio-optical feedbacks among phytoplankton, upper ocean physics and sea-ice in a global model, *Geophys. Res. Lett.*, 32, L05603, <https://doi.org/10.1029/2004GL020778>, 2005.
- Marsland, S. J., Haak, H., Jungclaus, J. H., Latif, M., and Roeske, F.: The Max-Planck-Institute global ocean/sea ice model with orthogonal curvilinear coordinates, *Ocean Model.*, 5, 91–126, 2002.
- Myriokefalitakis, S., Gröger, M., Hieronymus, J., and Döscher, R.: An explicit estimate of the atmospheric nutrient impact on global oceanic productivity, *Ocean Sci.*, 16, 1183–1205, <https://doi.org/10.5194/os-16-1183-2020>, 2020.
- Nakamoto, S., Prasanna Kumar, S., Oberhuber, J. M., Muneyama, K., and Frouin, R.: Chlorophyll modulation of sea surface temperature in the Arabian Sea in a mixed-layer isopycnal general circulation model, *Geophys. Res. Lett.*, 27, 747–750, <https://doi.org/10.1029/1999GL002371>, 2000.
- Nakamoto, S., Prasanna Kumar, S., Oberhuber, J. M., Ishizaka, J., Muneyama, K., and Frouin, R.: Response of the equatorial Pacific to chlorophyll pigment in a mixed layer isopycnal ocean general circulation model, *Geophys. Res. Lett.*, 28, 2021–2024, <https://doi.org/10.1029/2000GL012494>, 2001.
- NASA Goddard Space Flight Center, Ocean Ecology Laboratory, Ocean Biology Processing Group: Sea-viewing Wide Field-of-view Sensor (SeaWiFS) Chlorophyll Data, 2018 Reprocessing, NASA OB.DAAC [data set], <https://doi.org/10.5067/ORBVIEW-2/SEAWIFS/L3M/CHL/2018>, 2021a.
- NASA Goddard Space Flight Center, Ocean Ecology Laboratory, Ocean Biology Processing Group: Moderate-resolution Imaging Spectroradiometer (MODIS) Terra Chlorophyll Data; 2018 Reprocessing, NASA OB.DAAC [data set], <https://doi.org/10.5067/TERRA/MODIS/L3B/CHL/2018>, 2021b.
- NASA Goddard Space Flight Center, Ocean Ecology Laboratory, Ocean Biology Processing Group: Sea-viewing Wide Field-of-view Sensor (SeaWiFS) Downwelling Diffuse Attenuation Coefficient Data; 2018 Reprocessing, NASA OB.DAAC [data set], <https://doi.org/10.5067/ORBVIEW-2/SEAWIFS/L3M/KD/2018>, 2021c.
- Pacanowski, R. C. and Philander, S. G. H.: Parameterization of vertical mixing in numerical-models of tropical oceans, *J. Phys. Oceanogr.*, 11, 1443–1451, 1981.
- Paeth, H., Paxian, A., Sein, D. V., Jacob, D., Panitz, H. J., Warscher, M., Fink, A., Kunstmann, H., Breil, M., Engel, T., Krause, A., Tödter, J., and Ahrens, B.: Decadal and multi-year predictability of the West African monsoon and the role of dynamical downscaling, *Meteorol. Z.*, 26, 363–377, <https://doi.org/10.1127/metz/2017/0811>, 2017.
- Park, J. and Kug, J.: Marine biological feedback associated with Indian Ocean Dipole in a coupled ocean/biogeochemical model, *Clim. Dynam.*, 42, 329–343, <https://doi.org/10.1007/s00382-012-1640-5>, 2014.
- Park, J., Kug, J., Seo, H., and Bader, J.: Impact of bio-physical feedbacks on the tropical climate in coupled and uncoupled GCMs, *Clim. Dynam.*, 43, 1811–1827, <https://doi.org/10.1007/s00382-013-2009-0>, 2014a.
- Park, J.-Y., Kug, J.-S., and Park, Y.-G.: An exploratory modeling study on bio-physical processes associated with ENSO, *Prog. Oceanogr.*, 124, 28–41, <https://doi.org/10.1016/j.pocean.2014.03.013>, 2014b.

- Paulsen, H., Ilyina, T., Jungclaus, J. H., Six, K. D., and Stemmler, I.: Light absorption by marine cyanobacteria affects tropical climate mean state and variability, *Earth Syst. Dynam.*, 9, 1283–1300, <https://doi.org/10.5194/esd-9-1283-2018>, 2018.
- Paulson, C. A. and Simpson, J. J.: Irradiance Measurements in the Upper Ocean, *J. Phys. Oceanogr.*, 7, 952–956, 1977.
- Paxian, A., Sein, D. V., Panitz, H. J., Warscher, M., Breil, M., Engel, T., Tödter, J., Krause, A., Cabos, W., Fink, A., Ahrens, B., Kunstmann, H., Jacob, D., and Paeth, H.: Bias reduction in decadal predictions of West African monsoon rainfall using regional climate models, *J. Geophys. Res.-Atmos.*, 121, 1715–1735, <https://doi.org/10.1002/2015JD024143>, 2016.
- Ramesh, K. V. and Krishnan, R.: Coupling of mixed layer processes and thermocline variations in the Arabian Sea, *J. Geophys. Res.*, 110, C05005, <https://doi.org/10.1029/2004JC002515>, 2005.
- Ryabchenko, V. A., Gorchakov, V. A., and Fasham, M. J. R.: Seasonal dynamics and biological productivity in the Arabian Sea Euphotic Zone as simulated by a three-dimensional ecosystem model, *Global Biogeochem. Cy.*, 12, 501–530, 1998.
- Samson, G., Masson, S., Durand, F., Terray, P., Berthet, S., and Jullien, S.: Roles of land surface albedo and horizontal resolution on the Indian summer monsoon biases in a coupled ocean–atmosphere tropical-channel model, *Clim. Dynam.*, 48, 1571–1594, <https://doi.org/10.1007/s00382-016-3161-0>, 2017.
- Sattar, M. A., Kroeze, C., and Stokal, M.: The increasing impact of food production on nutrient export by rivers to the Bay of Bengal 1970–2050, *Mar. Pollut. Bull.*, 80, 168–178, 2014.
- Sein, D. V., Mikolajewicz, U., Gröger, M., Fast, I., Cabos, W., Pinto, J. G., Hagemann, S., Semmler, T., Izquierdo, A., and Jacob, D.: Regionally coupled atmosphere-ocean-sea ice-marine biogeochemistry model ROM: 1. Description and validation, *J. Adv. Model. Earth Syst.*, 7, 268–304, <https://doi.org/10.1002/2014MS000357>, 2015.
- Sein, D. V., Gröger, M., Cabos, W., Alvarez-Garcia, F. J., Hagemann, S., Pinto, J. G., Izquierdo, A., de la Vara, A., Koldunov, N. V., Dvornikov, A. Y., Limareva, N., Alekseeva, E., Martinez-Lopez, B., and Jacob, D.: Regionally coupled atmosphere-ocean-marine biogeochemistry model ROM: 2. Studying the climate change signal in the North Atlantic and Europe., *J. Adv. Model. Earth Syst.*, 12, e2019MS001646, <https://doi.org/10.1029/2019MS001646>, 2020.
- Seitzinger, S. P., Kroeze, C., Bouwman, A. F., Caraco, N., Dentener, F., and Styles, R. V.: Global patterns of dissolved inorganic and particulate nitrogen inputs to coastal systems: Recent conditions and future projections, *Estuaries*, 25, 640–655, 2002.
- Smith, W. O. and Sakshaug, E.: Polar Phytoplankton, in: *Polar Oceanography, part B: Chemistry, Biology, and Geology*, edited by: Walker Smith Jr., O., Academic Press, 477–525, <https://doi.org/10.1016/C2009-0-21623-0>, 1990.
- Steinacher, M., Joos, F., Frölicher, T. L., Bopp, L., Cadule, P., Cocco, V., Doney, S. C., Gehlen, M., Lindsay, K., Moore, J. K., Schneider, B., and Segschneider, J.: Projected 21st century decrease in marine productivity: a multi-model analysis, *Biogeosciences*, 7, 979–1005, <https://doi.org/10.5194/bg-7-979-2010>, 2010.
- Szabo, S., Nicholls, R. J., Neumann, B., Renaud, F. G., Matthews, Z., Sebesvari, Z., AghaKouchak, A., Bales, R., Ruktanonchai, C. W., Kloos, J., Foufoula-Georgiou, E., Wester, F., New, M., Rhyner, J., and Hutton, C.: Making SDGs Work for Climate Change Hotspots, *Environment: Science and Policy for Sustainable Development*, 58, 24–33, <https://doi.org/10.1080/00139157.2016.1209016>, 2016.
- Tangang, F., Chung, J. X., Juneng, L., Supari, S., Salimun, E., Ngai, S. T., Jamaluddin, A. F., Mohd, M. S. F., Cruz, F., Narisma, G., Santisirisomboon, J., Ngo-Duc, T., Van Tan, P., Singhruck, P., Gunawan, D., Aldrian, E., Sopaheluwakan, A., Grigory, N., Remedio, A. R. C., Sein, D. V., Hein-Griggs, D., McGregor, J. L., Yang, H., Sasaki, H., and Kumar, P.: Projected future changes in rainfall in Southeast Asia based on CORDEX–SEA multi-model simulations, *Clim. Dynam.*, 55, 1247–1267, <https://doi.org/10.1007/s00382-020-05322-2>, 2020.
- Taylor, K. E., Stouffer, R. J., and Meehl, G. A.: An overview of CMIP5 and the experiment design, *Bull. Am. Meteorol. Soc.*, 93, 485–498, 2012.
- Turco, M., Palazzi, E., von Hardenberg, J., and Provenzale, A.: Observed climate change hotspots, *Geophys. Res. Lett.*, 42, 3521–3528, 2015.
- Wu, R., Kirtman, B. P., and Pegion, K.: Surface latent heat flux and its relationship with sea surface temperature in the National Centers for Environmental Prediction Climate Forecast System simulations and retrospective forecasts, *Geophys. Res. Lett.*, 34, L17712, <https://doi.org/10.1029/2007GL030751>, 2007.
- Zhu, S., Remedio, A. R. C., Sein, D. V., Sielmann, F., Ge, F., Xu, J., Peng, T., Jacob, D., Fraedrich, K., and Zhi, X.: Added value of the regionally coupled model ROM in the East Asian summer monsoon modeling, *Theor. Appl. Climatol.*, 140, 375–387, <https://doi.org/10.1007/s00704-020-03093-8>, 2020.
- Zweng, M. M., Reagan, J. R., Antonov, J. I., Locarnini, R. A., Mishonov, A. V., Boyer, T. P., Garcia, H. E., Baranova, O. K., Johnson, D. R., Seidov, D., and Biddle, M. M.: *World Ocean Atlas 2013, Volume 2: Salinity*, edited by: Levitus, S., and Mishonov, A., NOAA Atlas NESDIS, 39 pp., 2013.